







Review

Landscape and Climate Changes in Southeastern Amazonia from Quaternary Records of Upland Lakes

José Tasso Felix Guimarães ^{1,*}, Prafulla Kumar Sahoo ^{1,2}, Pedro Walfir Martins e Souza-Filho ¹, Marcio Sousa da Silva ¹, Tarcísio Magevski Rodrigues ³, Edilson Freitas da Silva ¹, Luiza Santos Reis ⁴, Mariana Maha Jana Costa de Figueiredo ¹, Karen da Silva Lopes ¹, Aline Mamede Moraes ¹, Alessandro Sabá Leite ¹, Renato Oliveira da Silva Júnior ¹, Gabriel Negreiros Salomão ¹ and Roberto Dall'Agnol ¹

¹ Vale Institute of Technology, Rua Boaventura da Silva 955, Nazaré, Belém 66055-090, PA, Brazil

² Department of Environmental Science and Technology, Central University of Punjab, Bathinda 151401, India

³ Environment Management—Carajás Iron Ore Mining, North Ferrous Department, Estrada Raymundo Mascarenhas, S/N Mina de N4, Parauapebas 68516-000, PA, Brazil

⁴ Micropaleontology Laboratory, University of São Paulo, Rua do Lago, 562—Cidade Universitária, São Paulo 05508-080, SP, Brazil

* Correspondence: tasso.guimaraes@itv.org

Abstract: The upland lakes (ULs) in Carajás, southeastern Amazonia, have been extensively studied with respect to their high-resolution structural geology, geomorphology, stratigraphy, multielement and isotope geochemistry, palynology and limnology. These studies have generated large multiproxy datasets, which were integrated in this review to explain the formation and evolution of the ULs. These ULs evolved during the Pliocene–Pleistocene periods through several episodes of a subsidence of the lateritic crust (canga) promoted by fault reactivation. The resulting ULs were filled under wet/dry and warm/cool paleoclimatic conditions during the Pleistocene period. The multielement geochemical signature indicates that the detrital sediments of these ULs were predominantly derived from weathered canga and ferruginous soils, while the sedimentary organic matter came from autochthonous (siliceous sponge spicules, algae, macrophytes) and allochthonous (C3/C4 canga and forest plants and freshwater dissolved organic carbon) sources. Modern pollen rain suggests that even small ULs can record both the influence of canga vegetation and forest signals; thus, they can serve as reliable sites to provide a record of vegetation history. The integrated data from the sedimentary cores indicate that the active ULs have never dried up during the last 50 ka cal BP. However, subaerial exposure occurred in filled ULs, such as the Tarzan mountain range during the Last Glacial Maximum (LGM) and the Bocaína and S11 mountain ranges in the mid-Holocene period, due to the drier conditions. Considering the organic proxies, the expansion of C4 plants has been observed in the S11 and Tarzan ULs during dry events. Extensive precipitation of siderite in UL deposits during the LGM indicated drier paleoenvironmental conditions, interrupting the predominantly wet conditions. However, there is no evidence of widespread forest replacement by savanna in the Carajás plateau of southeastern Amazonia during the late Pleistocene and Holocene.

Keywords: Amazonia; upland lakes; Carajás mountain range; landscape evolution; Quaternary geology



Citation: Guimarães, J.T.F.; Sahoo, P.K.; e Souza-Filho, P.W.M.; da Silva, M.S.; Rodrigues, T.M.; da Silva, E.F.; Reis, L.S.; de Figueiredo, M.M.J.C.; Lopes, K.d.S.; Moraes, A.M.; et al. Landscape and Climate Changes in Southeastern Amazonia from Quaternary Records of Upland Lakes. *Atmosphere* **2023**, *14*, 621. <https://doi.org/10.3390/atmos14040621>

Academic Editor: Jason T. Ortegren

Received: 27 February 2023

Revised: 9 March 2023

Accepted: 11 March 2023

Published: 24 March 2023



Copyright: © 2023 by the authors. Licensee MDPI, Basel, Switzerland. This article is an open access article distributed under the terms and conditions of the Creative Commons Attribution (CC BY) license (<https://creativecommons.org/licenses/by/4.0/>).

1. Introduction

The upland lakes (ULs) in the Brazilian Amazon are singular mid-altitude (from 400 m to 800 m) landforms formed over iron and iron-aluminous lateritic crusts as a result of cyclic tectonic, weathering and the erosional processes under tropical climate conditions [1–3]. These lakes are classified as active and inactive lake systems, the latter corresponding to upland swamps [4].

The sediment deposition in ULs is highly influenced by the natural and local characteristics of the catchment basin, including the geology, vegetation cover, primary productivity of the central basin [5–7] and relative lake age [3]. Despite the relative homogeneity, the

drainage basins in southeastern Amazonia locally present various lithotypes and geomorphological settings. Consequently, they hold plant communities with different structures and compositions [8]. Moreover, diagenetic processes have modified sediment composition [5]. All of these factors have controlled the geochemical and limnological characteristics of these ULs over time [9,10].

The Quaternary deposits in Amazonian ULs have different thicknesses. Some display continuous sedimentation, as evidenced in the Seis Lagos (northwestern Amazonia), Maicuru/Maraconá (central-northeastern Amazonia) and Carajás (southeastern Amazonia) mountain ranges [4,11–18]. The investigations conducted at these localities have allowed an evaluation of the effects of the last glacial and interglacial periods on tropical Amazonia. ULs may become more similar to terrestrial habitats during the negative water balance period produced by prolonged water stress, which may affect the ecological attributes of water-dependent biota [19,20]. In contrast, more resilient ULs may act as microrefuges for such organisms. Thus, both the physical and biological aspects, as well as their dynamic nature, must be carefully evaluated over shorter (annual to decadal) and longer (century to millennial) time scales. In this review, we present the multiproxy dataset of the Quaternary surface and subsurface processes in the Carajás mountain range in southeastern Amazonia. We also use a series of multivariate statistical analyses to gain a better understanding of the differences/similarities between the ULs (Supplementary Data S1) [21–35].

Geology, Physiography and Climate

The study area is located in the eastern portion of Carajás Province, southeastern Amazonia (Figure 1), and the geology is represented by: (1) Mesoarchean tonalite–trondhjemite–granodiorite (TTG) series and granulitic units (Xikrin-Cateté Orthogranulite) [36,37]; (2) Neoarchean metavolcano-sedimentary sequences [38]; (3) Neoarchean intrusive rocks [39] and mafic–ultramafic stratified bodies [40]; (4) Paleoproterozoic sedimentary rocks [41]; and (5) Paleoproterozoic anorogenic intrusions [42].

The Cenozoic tropical paleoclimate has favored extensive weathering events in the region, contributing to the development of the lateritic crusts, which were mainly derived from metavolcano-sedimentary rocks, including the banded iron formation (BIF) of the Itacaiúnas Supergroup [1]. The ULs were formed according to neotectonic and weathering events that affected the lateritic crusts [1]. These lakes occur only at altitudes of between 600 and 800 m in the upper lateritic terrains (plateaus) of the Carajás mountain range, which includes Sul, Norte, Leste, Tarzan and Bocaína (Figure 1).

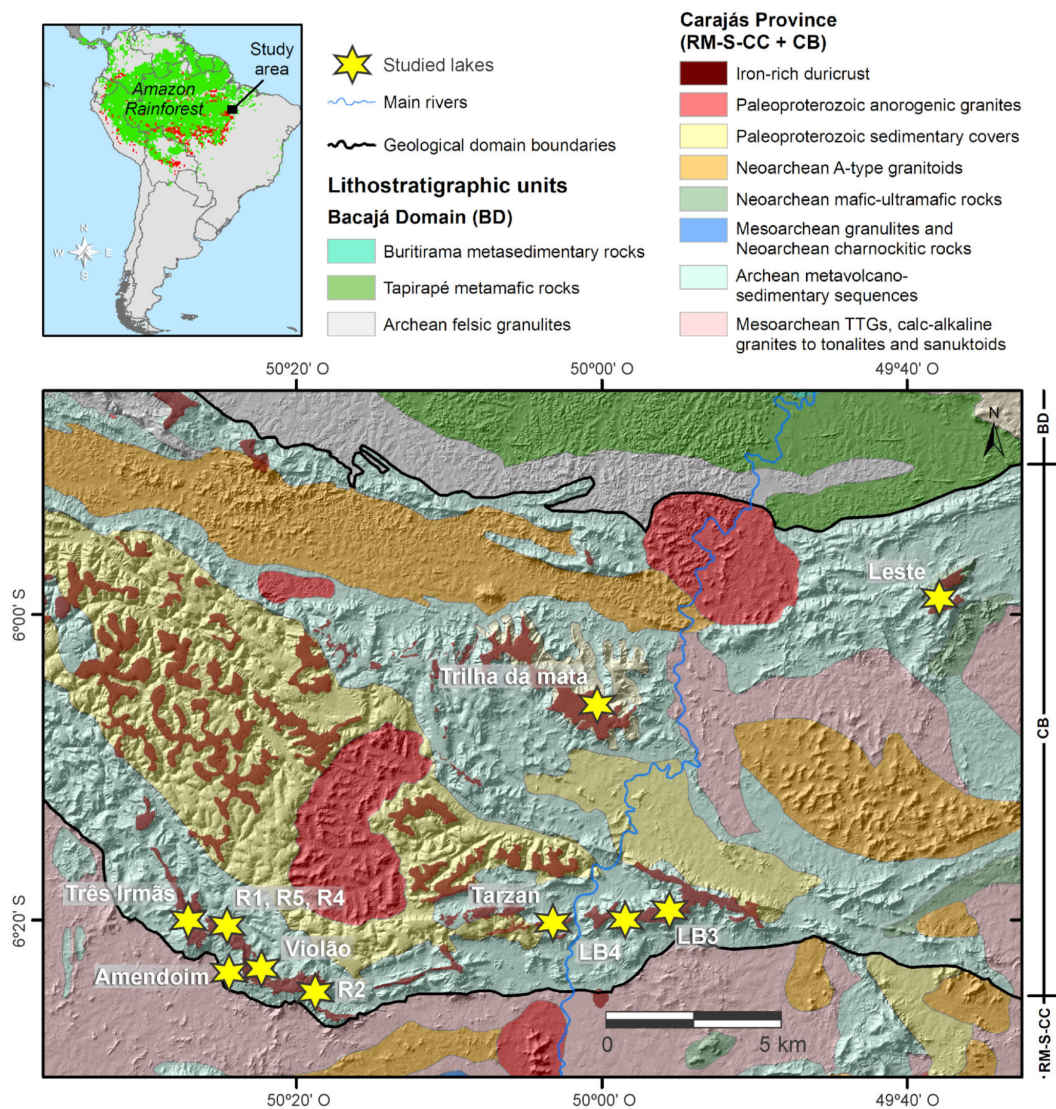


Figure 1. Upper map with study area in the context of South America and Amazon Rainforest (green area: forest cover, red areas: deforestation). Lower map with associated legends: geological map showing the main lithological units of the Carajás mountain range in the Brazilian Amazon. The studied lakes are located in the lateritic crusts in the Sul (active lakes: Três Irmãs, Amendoim, Violão; filled lakes: R1, R2, R4, R5), Norte (filled lake: Trilha da mata), Leste (active lake: lagoa Serra Leste—LSL), Tarzan (active lake: Tarzan) and Bocaína (filled lakes: LB3, LB4) plateaus; modified from [43]. Carajás Province (RM + S-CC + CB: Rio Maria + Sapucaia + Canaã dos Carajás domains + Carajás Basin).

The studied ULs are inserted into the Itacaiúnas River Watershed (IRW), which drains an area of approximately 41,300 km² [44] (Figure 1 and Table S1). These lakes are active or inactive (filled) depending on the sedimentary filling stage [16] (Table S1).

There are two well-defined seasons: a rainy season and a dry season [45]. The total rainfall varies between 1545 mm and 1863 mm during the rainy season (November to May) and between 159 mm and 321 mm during the dry season (June to October) [46]. The mean recorded temperature is 27.2 °C, with a minimum of 26.6 °C in January and a maximum of 28.1 °C in September [47].

2. Lake Formation Processes

The lateritic crusts of the Sul mountain range are displaced by sets of E–W faults that are responsible for the morphology of the plateaus, NW–SE normal faults to NE–SW frac-

tures, and sinistral—normal faults [3]. The partial dissolution of the lateritic crust oriented by these fractures and faults formed karst-like features, such as caves, sinkholes and underground streams [1]. A series of fault reactivations promoted the collapse of blocks along the normal faults, which formed the shallow upland lakes. The partial dissolution of the lateritic crust and intense run-off, particularly during the rainy season, favors the transport and deposition of clastic sediments into the lake [44] (Supplementary Video S1). In some cases, the overloading of the base of the lakes, together with fault reactivations, promoted new collapses and increased the accommodation space of the lakes [44] (Supplementary Video S1).

The shallow-water seismic transects and their reflection characteristics, as well as the sediment cores, allowed us to identify the geometry of the seismostratigraphic units deposited in the Carajás ULs [3] (Figure 2). The acoustic features are associated with the morphometry and morphology of the bedrock reflector, debris flows, synsedimentary deformational structures, plane-parallel reflectors and multiple reflectors from the water-substrate interface (Figure 2). The interface between the bottom sediments and the lateritic crust is marked by a total acoustic reflection of the crust, which produces strong-amplitude lake-bottom multiples (bedrock reflectors). The basal fine-grained deposits located near the main drainage inflows correspond to the fault-collapsed, basinward prograding clinofolds related to the delta fans. Underflow processes are responsible for carrying fine-grained particles toward the lake depocenter, interrupted by siderite beds. The top deposits are related to massive aggradational and structureless mud with some scattered peat fragments (Figure 2). This facies an arrangement that produces fining and thinning upward cycles, which might vary in thickness depending on the rate of the accommodation space.

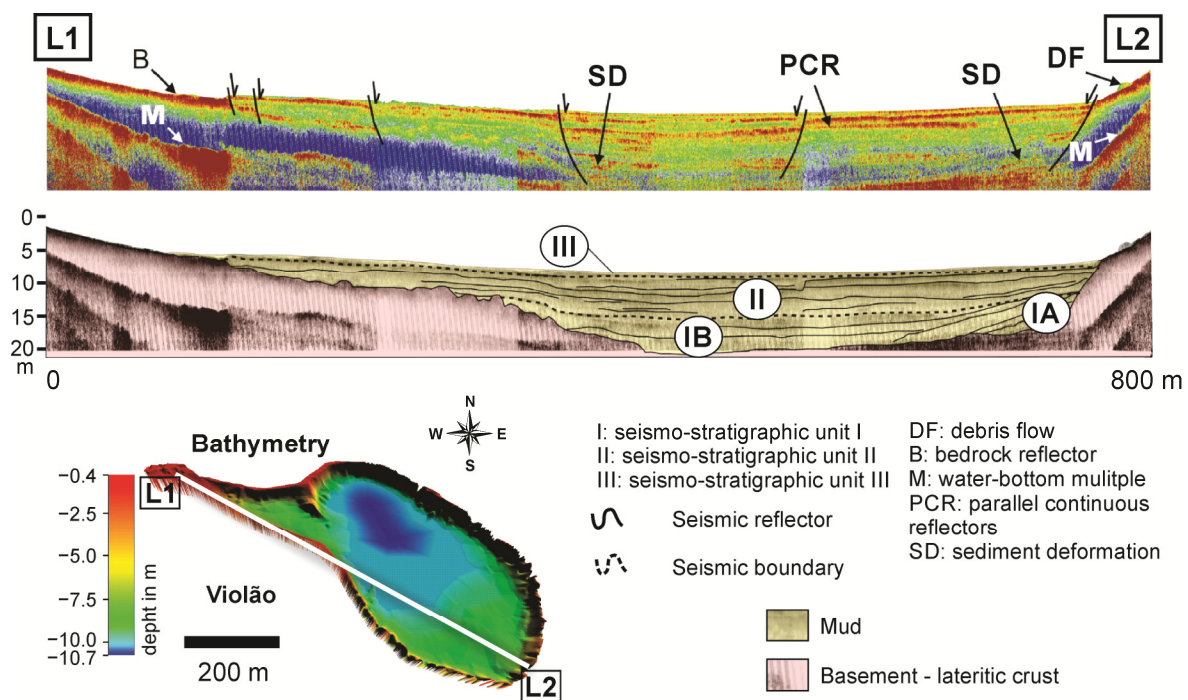


Figure 2. NW–SE longitudinal seismic transects showing the different observed morphologic levels, depositional units, basement and multiple reflectors, and fault. The seismostratigraphic interpretation in the lower part of the figure. All interpreted units can be accessed elsewhere [3]. Upper figure (shallow seismic image), middle figure (seismostratigraphic interpretation) and lower figure (legends and location of the seismic profile in the lake bathymetry).

3. Surface Geology and Geobotany of the Catchment Basins

The lateritic crusts of the study area are genetically classified as structured (iron ore), detrital and Al-rich crusts [48] (Figure 3). Structured and detrital crusts were formed by the lateritization of BIF and the weathering of the structured crusts, respectively, and

contain hematite, magnetite, goethite and secondarily quartz and clay minerals [9]. These crusts are generally thick and more resistant to modern weathering, forming only Petric Plinthosols/Petroferric Acrustox, which dominate the higher topographic levels. Conversely, the Al-rich crusts formed by the lateritization of mafic rocks are richer in clay minerals and gibbsite, especially close to the saprolite horizon. Additionally, they are less resistant to weathering and occur on lower quotas than structured and detrital crusts. Thus, these crusts may produce thicker soils (i.e., Ferrasols/Oxisols).

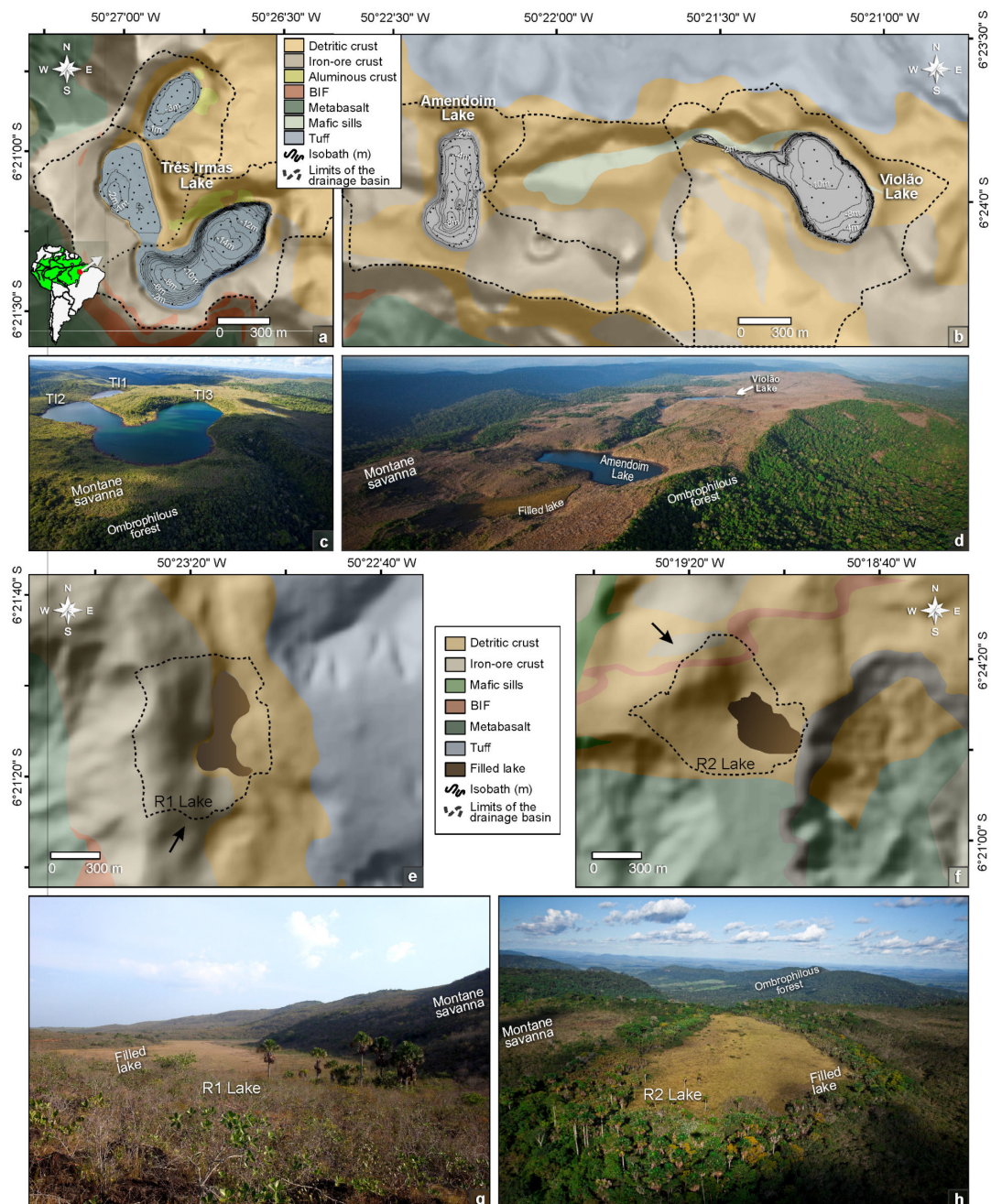


Figure 3. (a,b) Digital elevation model (DEM) integrated with bathymetric data showing the western and eastern portions of the Serra Sul Plateau and the main lithotypes described in the catchment basins of active ULs [25]. Aerial photograph of (c) Três Irmãs (TI1, TI2 and TI3), (d) Amendoim (AM) and Violão lakes (VL). (e,f) DEM showing the main lithotypes described in the catchment basins of filled ULs, also a detail (black arrow) for the direction of view of photo (e,f). (g,h) Aerial photograph of the filled ULs.

The detrital and structured crusts have some peculiar characteristics, including shallow, patchy and acidic soils, with low water retention and nutrient availability and high insolation and temperature [49,50], which allowed the widespread development of canga vegetation and hindered the colonization of tree species (Figure 3a–d), such as SDF and HETF [8,49]. This interpretation is supported by the high $\delta^{13}\text{C}$ values of the canga vegetation compared to soils in neotropical forests, which are related to more pronounced water shortages in cangas than forests [51]. Mafic sills and dikes are predominant on the slopes of the Carajás mountain range and marginal to the Três Irmãs and Violão lakes, extending toward Amendoim Lake (Figure 3a–d). Palms and macrophytes occur extensively in filled lakes (Figure 3e–h). Moreover, macrophytes, especially *Isoëtes cangae*, which is a very rare and endemic species, are widely found at the bottom of Amendoim Lake at depths up to 7 m [52]. The dominant plant species of each physiognomy are described in Table 1.

Table 1. Main plant species of canga vegetation, SDF (semideciduous tropical dry forests) HETF (humid evergreen tropical forest) and filled lakes according to their based on [9,30], reviewed according to Carajás Flora Project [53].

Vegetation Type	Species
Canga	<i>Dyckia duckei</i> (Bromeliaceae), <i>Ipomoea marabensis</i> (Convolvulaceae), <i>Erythroxyllum nelson-rosae</i> (Erythroxylaceae), <i>Bauhinia pulchella</i> , <i>Mimosa acutistipula</i> var. <i>ferrea</i> and <i>M. skinneri</i> var. <i>carajarum</i> (Fabaceae), <i>Byrsonima chrysophylla</i> (Malpighiaceae), <i>Norantea goyasensis</i> (Marcgraviaceae), <i>Tibouchina edmundoi</i> and <i>Pleroma carajasensis</i> (Melastomataceae), <i>Sobralia liliastrum</i> (Orchidaceae), <i>Axonopus carajasensis</i> , <i>Panicum millegrana</i> , <i>Paspalum cangarum</i> , <i>P. carajasense</i> and <i>Sporobolus multiramus</i> (Poaceae), <i>Borreria</i> (Rubiaceae), <i>Vellozia glauca</i> (Velloziaceae), <i>Callisthene microphylla</i> (Vochysiaceae).
SDF	<i>Licania blackii</i> (Chrysobalanaceae), <i>Aparisthium cordatum</i> and <i>Maprounea guianensis</i> (Euphorbiaceae), <i>Myrcia splendens</i> (Myrtaceae), <i>Henriettea ramiflora</i> , <i>Miconia chrysophylla</i> (Melastomataceae), <i>Matayba inelegans</i> (Sapindaceae).
HETF	<i>Tapirira guianensis</i> (Anacardiaceae), <i>Guatteria punctata</i> and <i>G. tomentosa</i> (Annonaceae), <i>Oenocarpus distichus</i> (Arecaceae), <i>Cordia sellowiana</i> (Boraginaceae), <i>Licania laxiflora</i> (Chrysobalanaceae), <i>Deguelia negrensis</i> , <i>Pseudopiptadenia suaveolens</i> (Fabaceae), <i>Emmotum nitens</i> (Icacinaceae), <i>Sacoglottis mattogrossensis</i> (Humiriaceae), <i>Mezilaurus itauba</i> (Lauraceae), <i>Miconia piperifolia</i> (Melastomataceae), <i>Myrcia silvatica</i> (Myrtaceae), <i>Neea ovalifolia</i> (Nyctaginaceae), <i>Matayba arborescens</i> (Sapindaceae), <i>Erismia uncinatum</i> (Vochysiaceae).
Filled lakes	<i>Mauritiella armata</i> (Arecaceae), <i>Eleocharis pedroviane</i> , <i>Cyperus</i> , <i>Scleria</i> (Cyperaceae), <i>Hydrochorea corymbosa</i> (Fabaceae), <i>Miconia alternans</i> (Melastomataceae), <i>Styrax griseus</i> (Styracaceae).

4. Modern Sedimentation Patterns: Basin Morphology and Source-to-Sink Relationship

The active Carajás ULs have mid-altitude ranges (695–725 m), very small surface areas (<0.5 km²), shallow to very shallow depths (<10 m: mean depth) and catchments with relatively high declivities (>20° and maximum of ~60°) [21]. The Violão (VL) and Amendoim (AM) lakes are separated by an intermediate basin that prevents any surface connection of water between them (Figure 3b). The catchment of Amendoim Lake was composed of two lakes (Figure 3d), but the smaller lake, located in the western portion, was progressively filled by detritic and organic sediments and currently represents a filled lake (swamp) colonized by macrophytes [30]. In contrast, the three lakes (TI1, TI2 and TI3) of Três Irmãs are connected, and the water flow follows the elevation gradient from TI1 to TI3 (Figure 3c), forming a small waterfall between the lakes [21].

The statistical distribution of the major and trace elements in the lake sediments (Table S3) shows that there is considerable variation in the chemical elements among the lakes, which is reinforced by the Kruskal–Wallis test (Table S4), which indicated *p* values of <0.05 for most of the elements. Si was the highest in VL and the lowest in TI2, which had the highest total organic carbon (TOC) values. The concentrations of Al, P, Ti and Zr are mainly enriched in TI1, followed by VL. This enrichment is due to the presence of Al-enriched lateritic crusts (including basalts) and soils. When compared to upper the continental crust (UCC) values, Fe is highly enriched in all of the lake sediments, followed

by P and Se, while the concentrations of Na, K and Ca are highly depleted. The strong depletion of these mobile elements is due to intense chemical weathering in the source areas, which is an indication of a typical lateritic environment.

Integrating the geochemical data from active ULs, based on principal components analysis (PCA), five major groups of geochemical associations are distinguished (Figure 4a), with the major detritic groups being similar to the catchment basin laterites [25]. The Ti-Zr-Hf-Y-Nb-HREE (Gp-1) corresponds to resistant minerals, which possibly remained stable during lateritization, while the different behavior of the LREE (Gp-2) relative to the HREE indicates their relative mobility during laterite formation and reprecipitation by REE-bearing minerals. The Al-Sc-V-Cr association (Gp-3) in the sediments reflects the signature of the local country rock, such as mafic sills. TOC-SO₃-Hg-Se (Gp-4) is controlled by organic matter, while the Fe-P-Mo-As-Zn (Gp-5) in the sediments is influenced by Fe-oxyhydroxide precipitation.

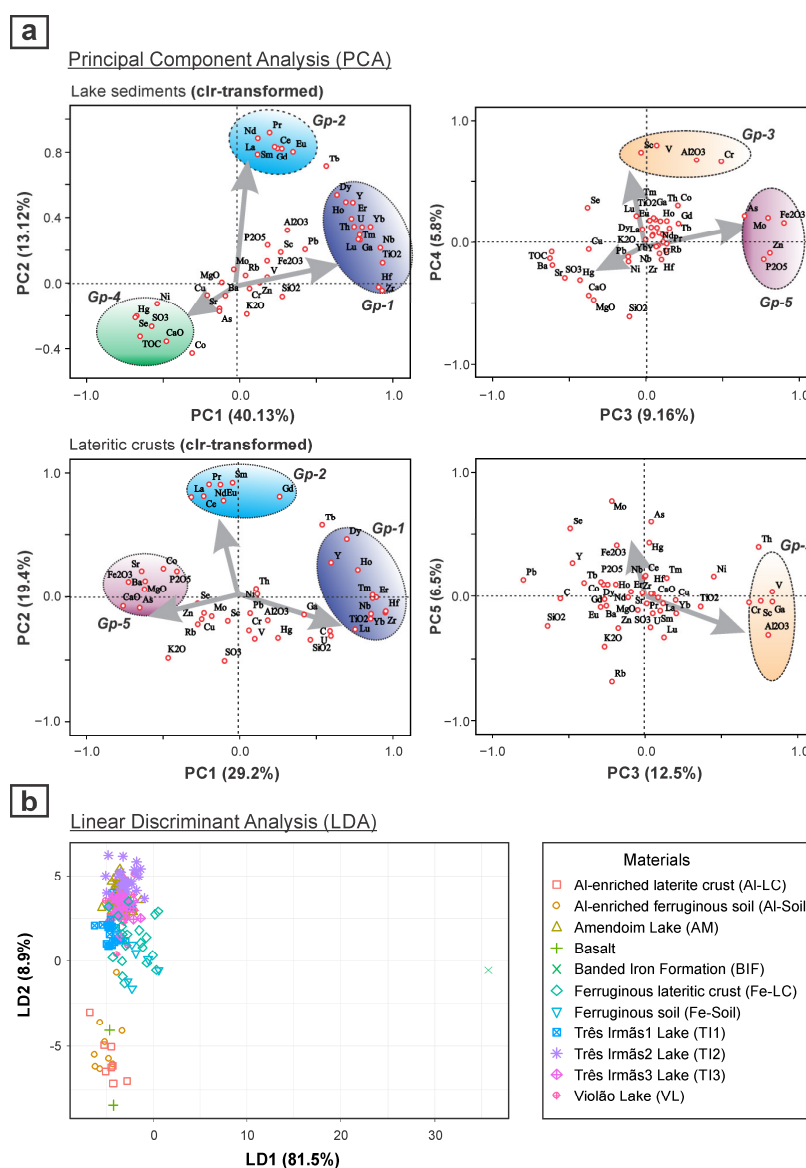


Figure 4. Principal component analysis (PCA) biplot of PC1 vs. PC2 and PC3 vs. PC4 for active lake sediments and catchment lateritic crusts [25], based on centered log-ratio (clr)-transformed data, showing the different geochemical associations and the major detrital signatures that are similar among them (a); and linear discriminate analysis (LDA) showing the distribution of lake sediments and the relationship with catchment basin materials (b).

The detritic association of Gps 1, 2 and 3, similar to the catchment rocks indicates a strong influence on the catchment basin lithology and laterization processes. The multivariate analysis, such as the linear discriminant analysis (LDA), further indicates that the detritic sediments are not directly derived from the parent rocks (Figure 4b), but are well correlated with the underlying weathered crusts (mainly ferruginous) and soils, while the ferruginous laterite crusts are the major source of detrital sediments. This inference demonstrates that lake sediments can be a potential tool for identifying and describing the catchment processes and basin lithology.

PCA performed on the centered log-ratio (clr)-transformed data was also employed to evaluate the relationships of the geochemistry of the bottom sediments among the filled lakes (Figures 5 and S1). The Bocaína (LB3 and LB4) lakes were mostly differentiated from the others as they loaded weakly positively on the PC2. This feature is related to the dominance in that area of Al-enriched lateritic crusts that were formed mostly from metavolcanic rocks. Thus, the geochemical signature of the Bocaína lake sediments shows higher concentrations of Al, Ga, Ti, Cr, V, Sc and REEs [24]. In these sediments, there is different geochemical behavior between the LREE and HREE, which is due to their different mobilities during lateralization [25]. Similar high enrichment of the detritic elements, such as Al, V, Ga and Cr, which are moderate to highly loaded on PC2, were also observed in the lakes from the Norte mountain range—Trilha da Mata Lake (LTM, LTP and LTD).

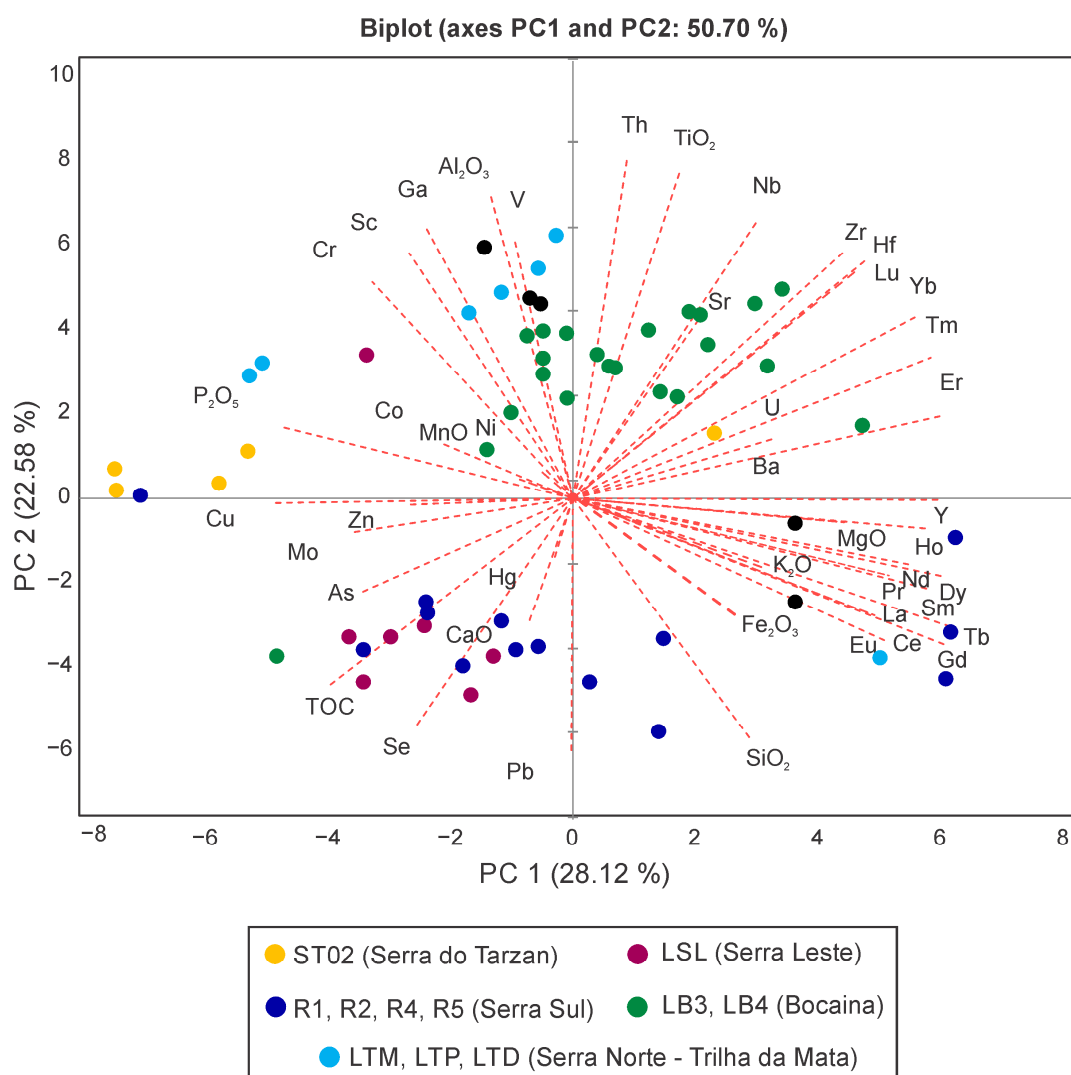


Figure 5. Principal component analysis (PCA) performed on centered log-ratio (clr)-transformed data for all filled lakes (sediment cores).

The sediments from Tarzan Lake (ST02) show mostly negative loading on PC1 and positive loading on PC2. This result is partly associated with Fe, suggesting that the crusts are similar to the Sul mountain range, but the high enrichment of Co, Cu, Mo, P, Cr and P in these sediments indicates a strong influence of mafic rocks, which is not exactly similar to that observed in the Bocaína lake sediments.

The sediments from Leste Lake (LSL) are negatively loaded on both PC1 and PC2 and seem very different from the sediments of the other lakes. The high enrichment of TOC in the detritic sediments of these lakes points to the control of different geomorphological and lithological characteristics of the basin. Moreover, in the Leste Lake sediments, As is more enriched, similar to the sediments from Tarzan lakes, suggesting the presence of sulfide minerals in the catchment rocks.

The filled lakes in the Sul mountain range (R1, R2, R4 and R5) have widely variable geochemical compositions, with the samples being positively and negatively loaded on PC1. Most of them are associated with Fe, as well as Si, thus indicating that the crusts developed mainly from iron formations, which have significant concentrations of Fe, while the Si contribution comes from BIF.

All of this fundamental knowledge of the modern lake sedimentary processes of Amazonian ULs and their catchment interactions can thus provide crucial insights for the interpretation of source—sink relationships and paleoclimate reconstruction.

5. Environmental Influences on Limnology and Water Quality

Regarding the ULs in the Carajás region, the lake waters are mostly acidic (avg. pH of 4.9–5.9), with high total Fe (up to 1.52 mg/L) and low SO_4^{2-} and other metal concentrations [10]. The low pH can be explained by the trivial level of carbonate minerals and the total dominance of ferruginous lateritic material in the catchment, as well as high sedimentary organic carbon in the lake bottom, which releases CO_2 and H_2S via bacterial decomposition, making the water acidic [54]. The high levels of Fe in the lake water are related to the weathering and erosion of the catchment ferruginous soils and lateritic crusts. This evidence indicates that the catchment geology is the dominant factor influencing the lake water chemistry.

These ULs are shallow, weakly stratified (Figure 6a) and classified as polymictic, which controlled the vertical mixing of the limnological parameters [10]. Although the water quality index (WQI) shows good water quality and high similarity among the studied lakes, the trophic state of these lakes varied significantly between ultraoligotrophic and eutrophic (Figure 6b), with lower values observed for Amendoim Lake [10]. High trophic states are due to nutrient concentrations, mainly total phosphorous (TP), promoting algal growth. The sources of TP for these lakes are associated with the presence of mafic rocks and caves with high guano volume [7,10]. Although Chl-a and cyanobacteria are mainly influenced by nutrients such as TP, this is not the case for these lakes; rather, they are controlled by additional factors, such as the seasonal climate conditions, catchment lithology specificities and lake morphology [10].

The Phytoplankton taxa in the lakes are characterized by small Chroococcales groups and desmids, together with filamentous algae, which are more commonly observed in the dry season. The Phytoplankton composition also varies among the lakes based on the differences in the water depth and nutrient concentration [10]. The studies conducted thus far have contributed to understanding the common limnological characteristics of the Amazonian ULs and their role in controlling the geochemical distribution of the elements and diagenetic processes in the sediments.

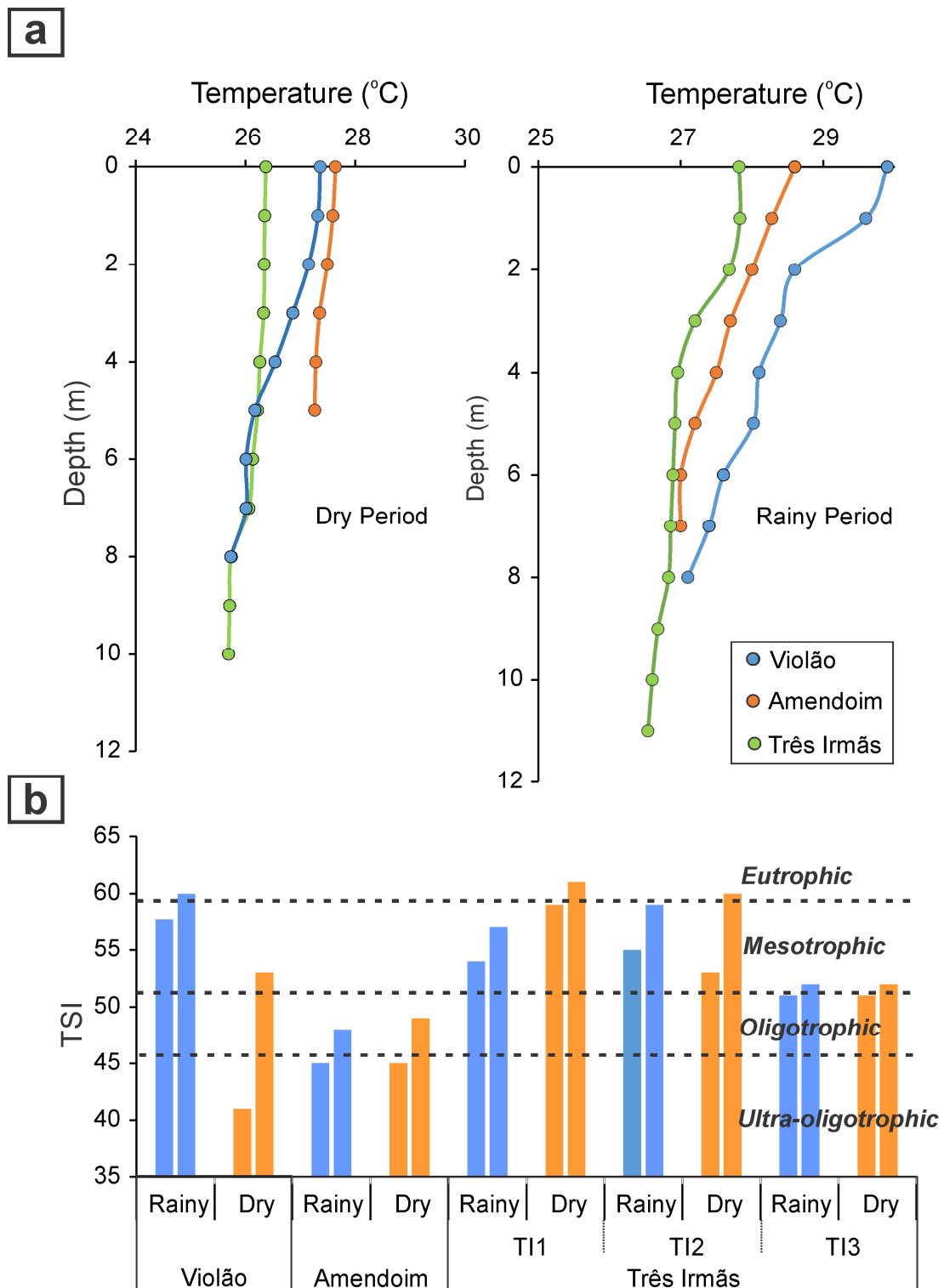


Figure 6. Vertical temperature profile in Violão, Amendoim and Três Irmãs lakes during the dry and rainy seasons showing the thermal stratification of the lakes (a), and trophic state index (TSI) of the lakes during both dry and rainy seasons (b), showing the significant variation in trophic state among lakes [10].

6. Role of Isotopes in Understanding the Sources of Sediment Organic Matter

The $\delta^{13}\text{C}$, $\delta^{15}\text{N}$ and C/N data from the surface sediments of Violão Lake indicate that the organic matter comes from siliceous sponge spicules, algae and C3 vascular forest

plants [5]. The latter is dominant in the shallower portion of this lake (arm), with more impoverished $\delta^{15}\text{N}$. In Amendoim Lake, the stable isotopic compositions are quite homogeneous and suggest organic sources composed of submerged macrophytes, including *I. cangae* and palms [6]. More diversified sources occur in the Três Irmãs Lake [9]. The isotopic and elemental signatures are indicative of C3 plants, macrophytes and freshwater dissolved organic carbon (DOC), while lake TI2 has a lower influence from aquatic organic matter, which is quite similar to the arm of Violão Lake, based on the $\delta^{15}\text{N}$ values (Figure 7a,b).

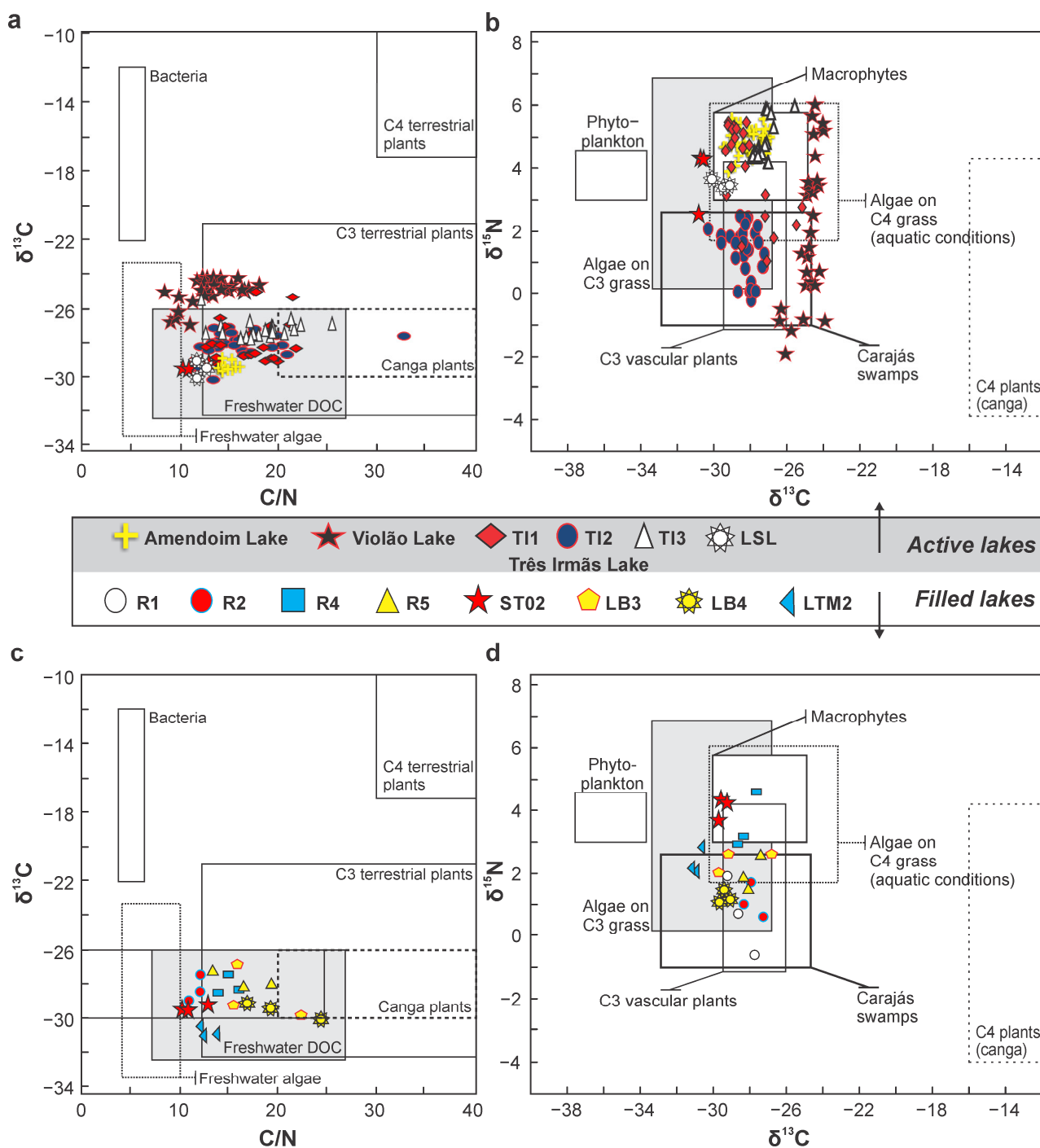


Figure 7. Binary plots of (a) $\delta^{13}\text{C}$ vs. C/N and (b) $\delta^{15}\text{N}$ vs. $\delta^{13}\text{C}$ of the surface sediments of the active ULs (modified from Sahoo et al., 2019), and (c) $\delta^{13}\text{C}$ vs. C/N and (d) $\delta^{15}\text{N}$ vs. $\delta^{13}\text{C}$ of sediment cores from filled ULs of the Carajás mountain range (fields based on [5–7,9,17,55–62]).

The filled lakes (R1, R2, R4, R5, ST02, LB3, LB4 and LTM2), are mainly composed of organic matter derived from freshwater DOC, C3 plants and algae, while canga plants are less represented or their signals are diluted by the other organic sources (Figure 7c,d). The enriched $\delta^{15}\text{N}$ values indicate a slightly higher aquatic influence on lakes R4 and ST02. More impoverished $\delta^{13}\text{C}$ values occur in LTM2. This site is located on a very narrow plateau with an area of approximately 0.033 km^2 surrounded by HETF [28]. The HETF has deeper soils with higher water availability than the lateritic crusts. Adaptations to seasonal droughts enable canga plants to withstand high water shortages, thus resulting in higher $\delta^{13}\text{C}$ values than HETF [51]. Thus, the signal from the HETF must be predominant in the sedimentary organic matter of lake LTM2. Therefore, the sources of organic matter to ULs are variable and are derived from the vegetation cover of the catchment and central basins, as well as lacustrine primary and secondary productivity [9,10].

7. Modern Pollen Rain Using UL Sediments

The edaphic conditions developed in the plateaus of the Carajás region lead to the formation of islands of canga plants that are structurally and compositionally different from the surrounding matrix [8,49]. The pollen signal of the HETF may overlap the signal of comparatively smaller savanna areas due to high production and enhanced dispersal capacity, but this is not always true.

The modern pollen rain of Violão Lake, evaluated using surface sediments, shows significant differences in its spatial distribution [29]. Pollen from canga vegetation is predominant in the lake, occurring in the eastern and western portions. Algae spores are mainly observed in the central portion of Violão Lake (Figure 2b), while pollen grains from the HETF and SDF are concentrated in its arm. This observed pattern is strongly associated with the occurrence of mafic rocks, where thicker soils and forest are developed. The comparative analysis between the floristic inventories of the catchment basin and modern pollen rain indicates that the pollen grains from canga plants are brought into the lake basin from 'regional' sources (outside the basin). In contrast, the pollen grains from HETF and SDF represent local sources (inside the basin), which reinforce the connection between mafic rocks and forest vegetation.

The modern pollen rain based in Amendoim Lake, located ~1 km eastward and 20 m below the mean altitude of Violão Lake (Figure 3b), shows that pollen grains from the HETF and SDF are dominant in surface sediments, despite the widespread abundance of canga plants in its drainage basin. This reinforces the role of topographic control and prevailing wind direction on pollen deposition [63].

Conversely, one year (2015–2016) of the pollen data collected from artificial traps installed along the drainage basin of Lake LTM2 did not indicate overlaps in the pollen signals between the vegetation types (Figure 8), although this lake is inserted in a HETF domain [28]. These findings, based on surface lake sediments and artificial traps, demonstrated that a clear savanna signal may also be acquired in sites with a reduced extent of this vegetation type.

Amendoim Lake is the only oligotrophic active lake in this region [7]. This trophic state favored the widespread development of *I. cangae*, which only occurs in this lake [52,64]. In addition, this species is very well represented in surface sediments by its microspores [63]. Thus, the use of *Isöetes* microspores as a proxy for low water levels and eutrophic and drier paleoclimatic conditions must be made with caution.

These studies improved our understanding of: (1) the ways modern pollen grains are transported into lakes; (2) the relationship between pollen and regional or local vegetation signals; and (3) the modern vegetation types, by considering a clear taxonomic and ecological determination, coupled with a robust pollen database of the studied site.

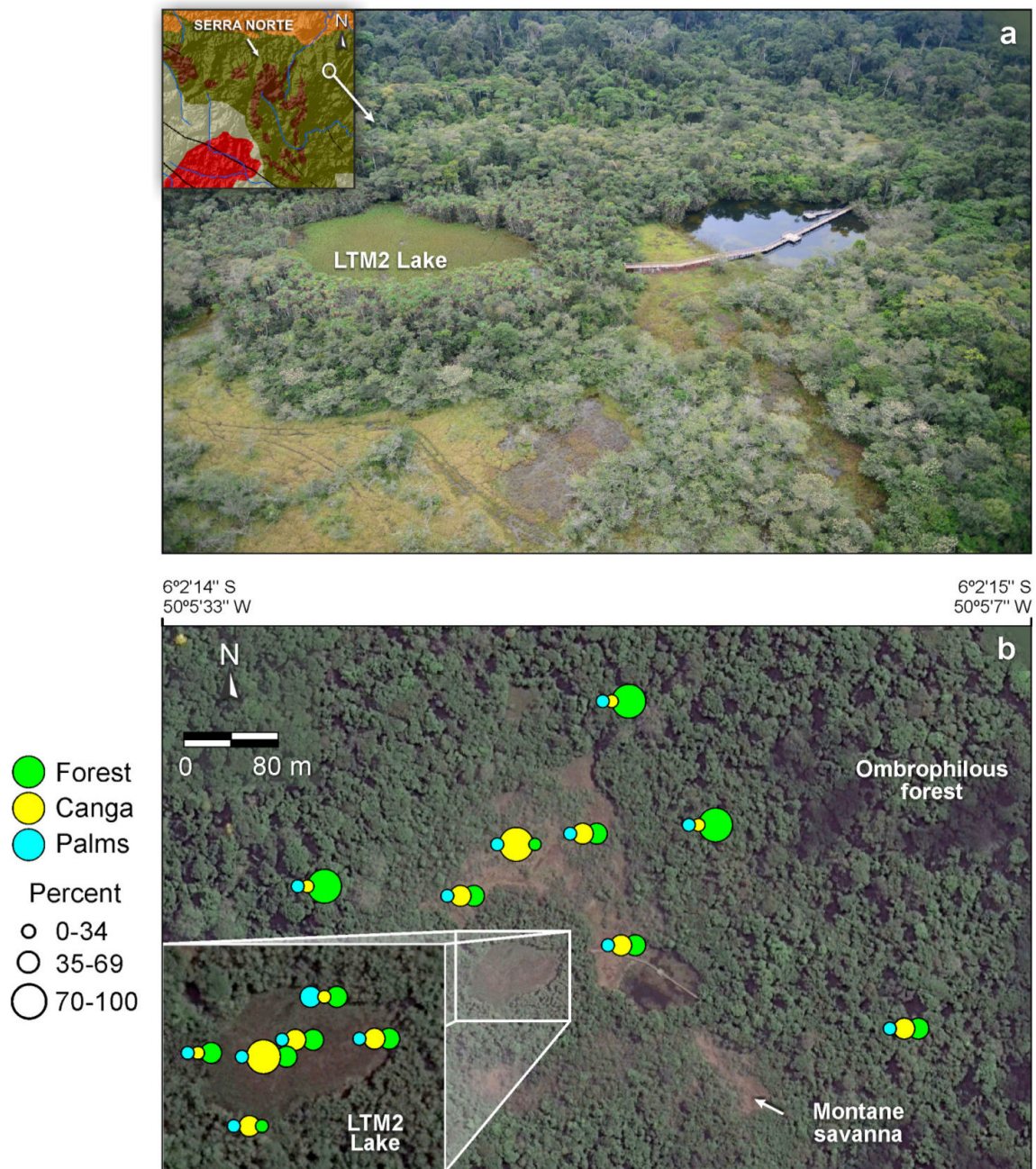


Figure 8. Modern pollen rain of the catchment basin of Lake LTM2 [28], Norte mountain range (a), showing the annual contribution (in %) of grains from forest, canga and palms (b).

8. UL Sediments: Implications for Paleovegetation and Paleoenvironmental Changes

Based on the sedimentary facies, geochemistry, pollen and spore analyses, as well as the carbon and nitrogen isotopes of the eleven sediment cores from the Carajás ULs, it was possible to understand the effects of hydroclimate changes on the geomorphological and limnological settings, as well as the vegetation dynamics of the southeastern Amazonia during the late Quaternary. Therefore, the absence of woody roots and physical or geochemical indicators of subaerial exposure indicate that these lakes have never dried up during the last 50 ka cal BP. Regarding the geochemical proxies (Figures S1 and 9), the detrital fraction (Al and Ti) provides insight into the climatic conditions that prevail in the source areas and the mechanisms involved in the transport of materials within the basin [16,17]. When the rainfall is strong enough, it can cause erosion and high detrital input to lakes [65], as shown

by the increase in Al and Ti. Ti and K are typically associated with clays, and an increase in the Ti/K suggests high amounts of weathered clay minerals deposited during high water stands and wetter periods [66]. In the plateau lakes of Carajás, Al/K and Ti/K show a strong correlation, and the slightly increased values seem to fit with Heinrich Stadials (HS) 1–3. This may be attributed to increased precipitation resulting from the strengthening of the South American summer monsoon due to a change in the Atlantic interhemispheric sea surface temperature (SST) gradient [67], which also affects the eastern Amazon. This increased precipitation interrupted a generalized drier period at the beginning of the Last Glacial Maximum (LGM) until approximately 13 ka cal BP (Figure 9). Carbon and nitrogen isotopes indicate a continuous predominance of C3 plants and freshwater DOC, except for Violão Lake, which presented more enriched values throughout the late Pleistocene, until 20 ka cal BP. This may be indicative of the presence of siderite nodules [4,16], which massively formed in Violão Lake at approximately 30 to 35 ka cal BP, and the presence of C4 plants in the drainage basin [17]. The multiproxy data from Saci Lake [68], located in southeastern Amazon Basin and 100 km from the Central Plateau of Brazil, have indicated a dry and cool climate between 35 and 18 cal yr BP, based on the high counts of open savanna taxa, *Podocarpus*, *Ilex*, as well as the low lake-level conditions indicated by *Sagittaria* and the low TOC content.

The high Al/K and Ti/K values imply a high amount of weathered clay minerals deposited during the high water stands and wetter period in the Holocene deposits of the active lakes, except for the relatively low ratios around the mid-Holocene (Figure 9). This will also be favored during the cycling of the dry-to-wet period. During dry periods, occasional rainfall leads to weathering, and these materials are transported during heavy rainfall events. Additionally, the pollen data from Leste Lake, which covered the last 15 ka cal BP, showed that canga vegetation and forests concomitantly contracted and expanded in a cyclic pattern during the last 5 ka cal BP. This is a clear indication of the predominance of strong millennial climate seasonality.

Filled lakes formed over structured and detrital (R1, R2, R4, R5) and Al-rich crusts (ST02, LB3, LB4, LTM2) are more influenced by the basin-filling effect. Thus, the establishment of modern swampy conditions (final filling stage) varies according to site. These conditions were attained in lakes R1, R5, ST02 and LTM2 at approximately 10 ka cal, while in lakes R2 and LB3, they were attained at 5 ka cal BP, and in lakes R4 and LB4 they were attained at 2 ka cal BP, which is observed from their TOC, carbon and nitrogen isotopic profiles (Figure 9). The detrital fraction of these cores follows the cycles of the lake-level and paleoclimate changes in the Carajás region, with good records for the LGM and mid-Holocene, as described by the relatively low Ti/K. However, in contrast to the active lakes, the Ti/K profiles between the late Quaternary deposits of the filled lakes cannot be compared as the latter were represented by modern swampy conditions. In other words, swamps are developed in lakes under very low accommodation space when the accommodation angle (measured between lake margins and depocenter) decreases at a point that restricts the deposition of detrital materials from the runoff to the lake margins.

Dryness with a subaerial exposure of lacustrine deposits was observed in lake ST02 during the LGM and in lakes LB3 and R2 during the mid-Holocene period. However, C4 plants were never predominant in the Carajás region, except for the LB3 area, which recorded canga expansion with C4 plants during the LGM, without siderite influence (Figure 9). Siderites were formed between ~35 and 30 ka cal BP in lakes R5 and ST02 and during the LGM in lakes R1 and R2. The Bocaína lakes do not present iron carbonates, such as siderite, which may be due to the different depositional conditions, as well as a lower abundance of Fe in the crust, which leads to a lower aqueous iron content [69,70]. The biomarker records from sediment cores collected in the Amazon River fan indicated that the Amazon basin have not shown C3/C4 vegetation replacements during the last 50 ka BP [71,72].

Cool-adapted taxa were widely developed in the Carajás region and occurred throughout the late Pleistocene, until ~7 ka cal, with a higher abundance observed before 40 ka cal

BP. Most of the LGM deposits were not suitable for high pollen concentrations due to the sediment redox conditions, which are influenced by diagenetic changes, except for lake LB3, which recorded a higher abundance of cool-adapted taxa during the LGM.

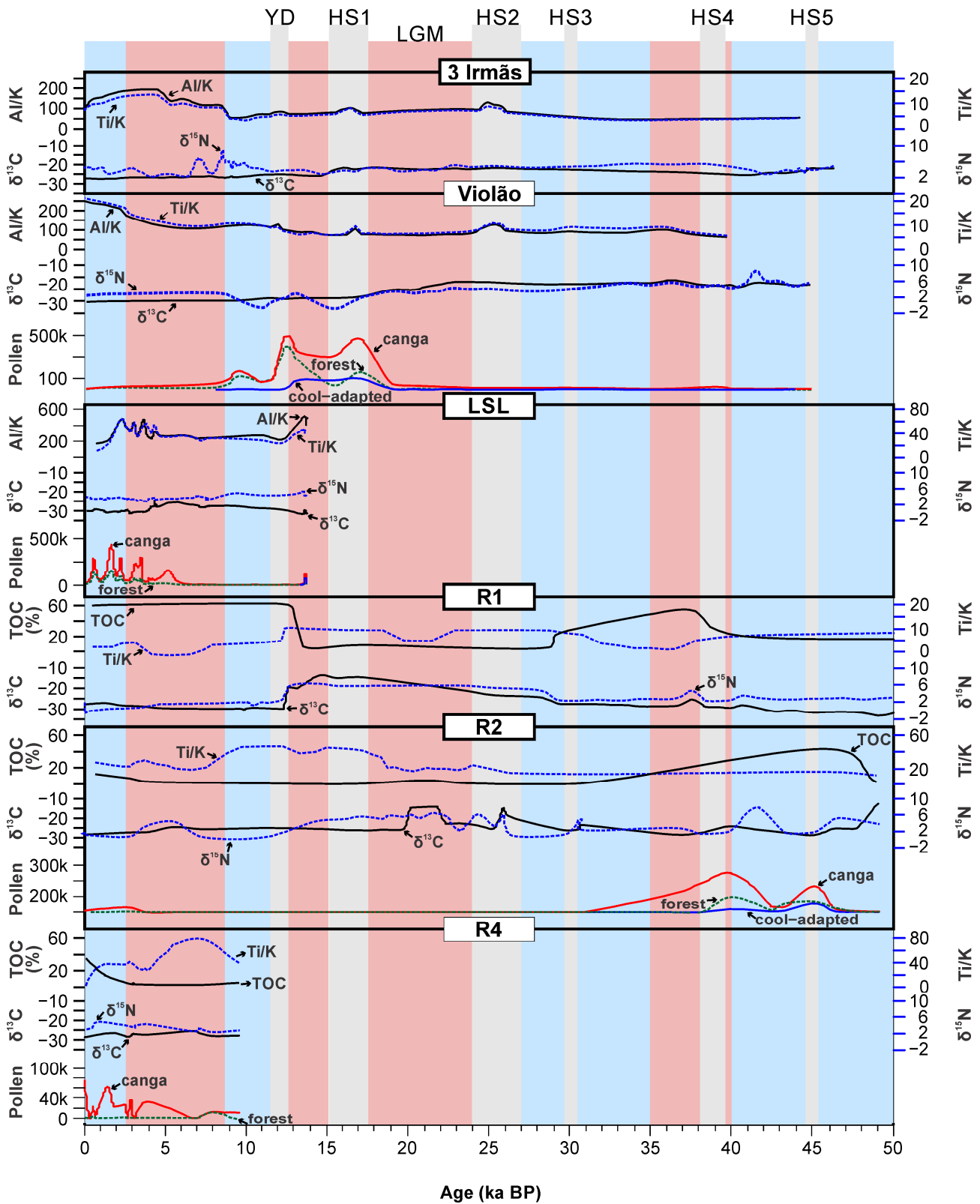


Figure 9. Cont.

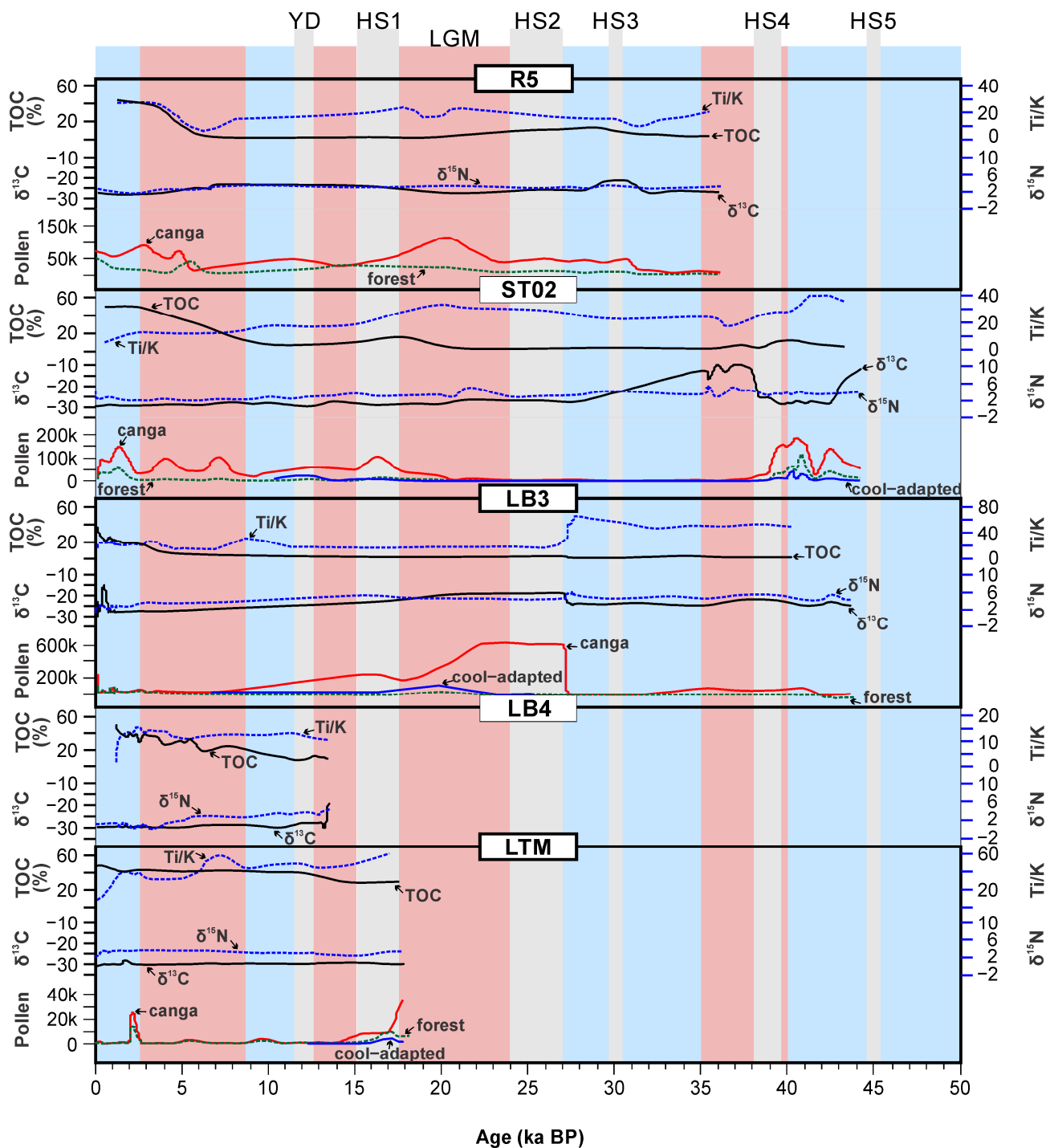


Figure 9. Generalized profile of the geochemical (Al/K and TOC with black line, Ti/K with blue-dashed line), isotopic ($\delta^{13}\text{C}$ with black line, $\delta^{15}\text{N}$ with blue dashed line), and pollen (canga vegetation with red line, forest with green dashed line and cool-adapted taxa with blue line) data of active (Três Irmãs, Violão and Serra Leste) and filled (R1, R2, R4, R5, ST02, LB3, LB4 and LTM) lakes. Light blue and red vertical bars represent wet and dry lacustrine phases in the ULs of Carajás [4,13,16,17,26,27]. Divided into 2 parts. YD (Younger Dryas), HS (Heinrich event) and LGM (Last Glacial Maximum).

The interpretation of the speleothem data from Paraíso cave in the eastern Amazonia indicates wetter climate conditions than those present at ~6 ka cal BP [73]. This contradicts a long set of paleoclimate studies in the Carajás region that indicate the dominance of montane savanna and SDF during the mid-Holocene period under drier climatic

conditions [4,13,16,18,26,27,74–76]. Smith et al. [77] proposed that the Holocene pollen assemblage of Carajás only reflects canga vegetation with small signals from the HETF, thus reflecting local changes on the plateau and making it difficult for any regional-scale vegetation changes. Smith et al. [77] based their assumptions on the modern pollen rain of Violão Lake [29], while the modern pollen rain of Amendoim Lake shows the opposite pattern, with a predominance of the pollen signal from the HETF [30]. Thus, it depends on the topographic position of each lake and wind direction, among other factors [63]. Therefore, the multiproxy data from several cores from active and filled lakes must be used to better indicate the paleoclimatic changes throughout this region.

The drier conditions during the mid-Holocene period in Carajás are mainly based on the multielemental and organic isotope geochemistry, with strong indications of water deficits and low weathering and sedimentation rates [4,13,16,17,27,75]. In addition, lakes LB3 and R2 (~40 km from each other) were subaerially exposed during this period, with massive formations of iron oxides and mud cracks (Figure S1). The drier mid-Holocene event was widespread along the southern tropics [75,78–82] and according to the numerical simulations [83]. The pollen and geochemical records of Saci Lake indicated that between 7.5 and 5 ka cal BP, open savanna and the SDF taxa expanded in the region, suggesting a short-scale dry event [68]. This may be a consequence of the low insolation, which induced a less effective land–sea contrast, reducing the South Atlantic Convergence Zone intensity and weakening the SAMS [82,83].

9. Current Approach and Future Perspectives of Paleoenvironmental Studies in Carajás

The large number of pollen and geochemical datasets generated thus far in the Carajás region on the vegetation dynamics and landscape evolution associated with human and natural forces has naturally led to the resolution of scientific questions, such as whether the forest was replaced by savanna in the eastern portion of the Amazon basin, which for a long time remained unanswered. However, although pollen analysis is a fundamental tool in paleoenvironmental studies, the limitations in species-level identification hamper broader discussions about the dynamics of plant communities, leading to biases in pollen-based climate reconstructions. Poaceae, for instance, is one of the most problematic taxa, as it is abundant in fossil records and commonly used as an indicator of vegetation openness due to dry climatic conditions [74,84]. The association of Poaceae with dry environments, however, must be evaluated with caution, as some species can also be found in flooded and swamp areas [63]. Therefore, only species-level identification makes it possible to distinguish among the species adapted to water stress conditions on cangas from those that inhabit swampy environments.

A very promising tool that would improve the reconstruction of past flora and move beyond measures of the presence-absence of species in natural systems is environmental DNA (eDNA) [85,86]. Any given sample (e.g., root, leaves, fruit, pollen) contains eDNA, which is continuously deposited in the environment in ways that enable the reconstruction of ecological and evolutionary processes [87]. By extracting these pieces of information, the rate of discovery would accelerate as no a priori information about the likely species found in a particular environment is required to identify those individuals [87]. Moreover, even trace samples of eDNA left behind by plants and animals that are no longer present in the environment can persist for centuries or millennia in soils and lake sediments and remain detectable [88–90]. Thus, the use of eDNA analysis is very well suited for studies that require multiple species detection, such as surveys of past vegetation and of community diversity dynamics through time [90,91].

The current barriers to the use of eDNA include the need for extensive training in molecular biology and the subsequent analysis of the genetic data [87]. The rapid emergence of commercial companies specializing in eDNA, however, tends to overcome such shortcomings.

Through the identification of plant species and the knowledge of the geographic and altimetric distribution range of those species, a pollen-based temperature is likely to be obtained [92], thus allowing inferences about the changes in temperature over time. Although a consolidated method is available in the literature [93], such approaches are still very incipient and overlooked in paleoenvironmental studies carried out in continental environments such as lakes and oxbows.

Paleotemperature reconstructions and paleoprecipitation records obtained from compound-specific isotope analysis [94,95] are also underexplored in paleoenvironmental studies in Amazonia. Nevertheless, they are fundamental tools for understanding the effects of environmental changes on the distribution and composition of the plant community [18]. Therefore, we highlight the importance of using these proxies, together with pollen and geochemistry, to obtain more robust and accurate interpretations of past environmental and climatic changes in the Amazon region.

A more achievable short-term goal is the potential use of guano deposits as environmental archives, with, for example, applications for biodiversity and wildlife conservation, as well as ecological networks, rather than only general discussions about vegetation dynamics.

More than 1500 small cavities have already been identified in Carajás, considered one of the largest concentrations of caves in Brazil [96]. Guano deposits are very common in these cave systems, and several meters of bat guano can accumulate on cave floors [97], representing an outstanding environmental archive. However, although such an approach is incipient in Brazil, an increasing number of studies worldwide have shown that bat guano deposits provide valuable information and may track changes in humidity, precipitation, and local vegetation over millennial timescales [98–101]. Future investigations should address paleoenvironmental and paleoecological studies from this new perspective to unravel the ecological interactions between animals and vegetation as drivers of temporal and spatial changes in the landscape.

10. Conclusions

This review presents an integrated interpretation of a large multiproxy dataset to clarify some key questions about the formation of the Carajás ULs, as well as the apparent mismatches in the plant and paleoclimate dynamics during the last 50 ka cal BP. The ULs were formed by structural processes and the dissolution of lateritic crusts during the late Cenozoic period, and sedimentation possibly started during the Quaternary. Detritic facies are related to predominant chemical weathering, peat facies to water-saturated conditions and high primary productivity or macrophyte development to ultraoligotrophic conditions, depending upon the accommodation space. The cyclical pattern of sediment deposition with alternating beds of mud, peat and siderites reveals that the paleoclimate seasonality was stronger during the Holocene than late Pleistocene period, which was evidenced by the stratigraphy, multi-elemental and isotope geochemistry and the pollen data. The ULs were strongly influenced by the drier paleoclimate conditions of the LGM and mid-Holocene period, with very low detrital inflow, the subaerial exposure of lake deposits and the widespread formation of siderites (late Pleistocene). However, there is no sign of widespread forest replacement by savanna during the studied period. Despite the strong edaphic control on the vegetation distribution in Carajás, paleoenvironmental studies based on multi-proxy approaches have shown that the pollen records retrieved from the ULs reflect the response of plant communities to changes in the climatic conditions (local or regional). Finally, we emphasize that future studies in Amazonia should investigate past ecological interactions and their role in landscape evolution, as well as making use of the very promising, but still underused, techniques, such as eDNA and paleotemperature reconstructions. Therefore, this study brings a new outlook to paleoenvironmental studies.

Supplementary Materials: The following supporting information can be downloaded at: <https://www.mdpi.com/article/10.3390/atmos14040621/s1>. Data S1. Summary of the research methods that supported the different research areas comprising the ‘Paleoclimate Project’, which is the first-ever large-scale survey undertaken by Instituto Tecnológico Vale in upland lakes of the Carajás region. Table S1. General description of the surface sediment samples and sediment cores collected from the upland lakes of the Carajás region. Table S2. Radiocarbon dates (AMS) of the samples from the Carajás region. Table S3. Analytical data of surface lake sediments (Violão (VL), Amendoim (AM) and Três Irmãs (TI1, TI2, TI3) and catchment basin rocks and soils, and core lake sediments (R1, R2, R4, R5, LB1, LB2, LB3, LB4, ST02, LSL, LTD, LTM) Carajás, Brazil. Units: major and minor elements (Si to TS) in %; trace and REEs in mg/kg. Table S4. Kruskal–Wallis test results of the chemical parameters among grouping variables (lakes). Units: major and minor elements (Si to TS) in %; trace and REEs in mg/kg. Figure S1. (a) Graphic sedimentary log of the active lakes: LTI3 (Três Irmãs-S11), VL2 (Violão-S11), LSL (Serra Leste) and inactive lakes: R1, R2, R4 and R5 (S11). (b) Graphic sedimentary log of the inactive lakes: ST2 (Serra do Tarzan), LB3 and LB4 (Serra da Bocaína), LTM2 (Lagoa Trilha da Mata-Serra Norte). Video S1. Tectono-sedimentary evolution model of the upland Violaão Lake and its relationship with reactivation of collapse normal faults and sedimentary infilling.

Author Contributions: J.T.F.G., P.K.S. and P.W.M.e.S.-F. contributed to the conceptualization, data curation, formal analysis, original draft and review and editing; M.S.d.S., T.M.R. performed the formal analysis and provided resources; E.F.d.S., L.S.R., M.M.J.C.d.F., K.d.S.L., A.M.M. and A.S.L. worked on formal analysis; R.O.d.S.J., G.N.S. and R.D. supervised and worked on the review and editing. All authors have read and agreed to the published version of the manuscript.

Funding: This study was funded by Instituto Tecnológico Vale (RBRS000603.05.02.PC06, R100603.FA.06), CNPq (479182/2012-4; 442088/2014-0) and FAPESPA (2017/04994-1). The first (J.T.F.G.), third (P.W.M.e.S.-F) and last (R.A.) authors were supported by CNPq through research scholarships (306767/2019-8, 310283/2019-1, 304648/2019-1, respectively).

Institutional Review Board Statement: Not applicable.

Informed Consent Statement: Not applicable.

Data Availability Statement: Not applicable.

Acknowledgments: The authors are thankful to the members of DIPE, DIFN, S11D of Vale S.A. for field support and scientific discussions. This project was carried out in the National Forest of Carajás under permission of IBAMA (SISBIO 35594-2). The content of the manuscript has previously appeared online as a preprint [26].

Conflicts of Interest: The authors declare that the research was conducted in the absence of any commercial or financial relationships that could be construed as a potential conflict of interest. The authors declare no conflict of interest.

References

1. Maurity, C.W.; Kotschoubey, B. Evolução recente da cobertura de alteração no platô N1-Serra dos Carajás-PA: Degradação, pseudocarstificação, espeleotemas. *Bol. Mus. Para. Emilio Goeldi. Ser. Ciênc. Terra* **1995**, *7*, 331–362.
2. Costa, M.L.; Carmo, M.S.; Behling, H. Mineralogia e geoquímica de sedimentos lacustres com substrato laterítico na Amazônia Brasileira. *Rev. Bras. Geociências* **2005**, *35*, 165–176. [[CrossRef](#)]
3. Souza-Filho, P.W.M.; Pinheiro, R.V.L.; Costa, F.R.; Guimarães, J.T.F.; Sahoo, P.K.; Silva, M.S.; Silva, C.G. The role of fault reactivation in the development of tropical montane lakes. *Earth Surf. Process. Landforms* **2020**, *45*, 3732–3746. [[CrossRef](#)]
4. Reis, L.S.; Guimarães, J.T.F.; Souza-Filho, P.W.M.; Sahoo, P.K.; Figueiredo, M.M.J.C.; Souza, E.B.; Giannini, T.C. Environmental and vegetation changes in southeastern Amazonia during the late Pleistocene and Holocene. *Quat. Int.* **2017**, *449*, 83–105. [[CrossRef](#)]
5. Sahoo, P.K.; Souza-Filho, P.W.; Guimarães, J.T.; Da Silva, M.S.; Costa, F.R.; De Oliveira Manes, C.L.; Oti, D.; Júnior, R.O.; Dall’Agnol, R. Use of multi-proxy approaches to determine the origin and depositional processes in modern lacustrine sediments: Carajás Plateau, Southeastern Amazon, Brazil. *Appl. Geochem.* **2015**, *52*, 130–146. [[CrossRef](#)]
6. Sahoo, P.K.; Guimaraes, J.T.; Souza-Filho, P.W.; da Silva, M.S.; Maurity, C.W.; Powell, M.A.; Rodrigues, T.M.; Da Silva, D.F.; Mardegan, S.F.; Neto, A.E.; et al. Geochemistry of upland lacustrine sediments from Serra dos Carajás, Southeastern Amazon, Brazil: Implication for catchment weathering, provenance, and sedimentary processes. *J. South Am. Earth Sci.* **2016**, *72*, 178–190. [[CrossRef](#)]

7. Sahoo, P.K.; Guimarães, J.T.; Souza-Filho, P.W.M.; Da Silva, M.S.; Júnior, R.O.S.; Pessim, G.; De Moraes, B.C.; Pessoa, P.F.; Rodrigues, T.M.; Da Costa, M.F.; et al. Influence of seasonal variation on the hydro-biogeochemical characteristics of two upland lakes in the Southeastern Amazon, Brazil. *An. Acad. Bras. Ciências* **2016**, *88*, 2211–2227. [[CrossRef](#)]
8. Nunes, J.A.; Schaefer, C.E.G.R.; Ferreira Júnior, W.G.; Neri, A.V.; Correa, G.R.; Enright, N.J. Soil-vegetation relationships on a banded ironstone 'island', Carajás Plateau, Brazilian Eastern Amazonia. *An. Acad. Bras. Ciênc.* **2015**, *87*, 2097–2110. [[CrossRef](#)] [[PubMed](#)]
9. Sahoo, P.K.; Guimarães, J.T.; Souza-Filho, P.W.; da Silva, M.S.; Júnior, W.N.; Powell, M.A.; Reis, L.S.; Pessenda, L.C.; Rodrigues, T.M.; da Silva, D.F.; et al. Geochemical characterization of the largest upland lake of the Brazilian Amazonia: Impact of provenance processes. *J. South Am. Earth Sci.* **2017**, *80*, 541–558. [[CrossRef](#)]
10. Sahoo, P.K.; Guimarães, J.T.; Souza-filho, P.W.; Bozelli, R.L.; de Araujo, L.R.; de Souza Menezes, R.; Lopes, P.M.; da Silva, M.S.; Rodrigues, T.M.; da Costa, M.F.; et al. Limnological characteristics planktonic diversity of five tropical upland lakes from Brazilian Amazon. *Ann. Limnol. Int. J. Limnol.* **2017**, *53*, 467–483. [[CrossRef](#)]
11. Colinvaux, P.A.; Irion, G.; Räsänen, M.E.; Bush, M.B.; Nunes de Mello, J.A.S. A paradigm to be discarded: Geological and paleoecological data falsify the HAFER & PRANCE refuge hypothesis of Amazonian speciation. *Amazoniana* **2001**, *16*, 609–646.
12. Bush, M.B.; Oliveira, P.E.; Colinvaux, P.A.; Miller, M.C.; Moreno, J.E. Amazonian palaeoecological histories: One hill three watersheds. *Palaeogeogr. Palaeoclimatol. Palaeoecol.* **2004**, *214*, 359–393. [[CrossRef](#)]
13. Sifeddine, A.; Martin, L.; Turcq, B.; Volkmer-Ribeiro, C.; Soubiès, F.; Cordeiro, R.C.; Suguio, K. Variations of the Amazonian rainforest environment: A sedimentological record covering 30,000 years. *Palaeogeogr. Palaeoclimatol. Palaeoecol.* **2001**, *168*, 221–235. [[CrossRef](#)]
14. Cordeiro, R.; Turcq, B.; Sifeddine, A.; Lacerda, L.; Filho, E.S.; Gueiros, B.; Potty, Y.; Santelli, R.; Pádua, E.; Patchinelam, S. Biogeochemical indicators of environmental changes from 50Ka to 10Ka in a humid region of the Brazilian Amazon. *Palaeogeogr. Palaeoclimatol. Palaeoecol.* **2011**, *299*, 426–436. [[CrossRef](#)]
15. D'Apolito, C.; Absy, M.L.; Latrubesse, E.M. The Hill of Six Lakes revisited: New data and re-evaluation of a key Pleistocene Amazon site. *Quat. Sci. Rev.* **2013**, *76*, 140–155. [[CrossRef](#)]
16. Guimarães, J.T.F.; Sahoo, P.K.; Souza-Filho, P.W.M.; Maturity, C.W.; Silva, J.R.O.; Costa, F.R.; Dall'Agnol, R. Late Quaternary environmental climate changes registered in lacustrine sediments of the Serra Sul de Carajás southeast Amazonia. *J. Quat. Sci.* **2016**, *31*, 61–74. [[CrossRef](#)]
17. Guimarães, J.T.F.; Sahoo, P.K.; De Figueiredo, M.M.J.C.; Lopes, K.S.; Gastauer, M.; Ramos, S.J.; Caldeira, C.F.; Souza-Filho, P.W.M.; Reis, L.S.; Da Silva, M.S.; et al. Lake sedimentary processes and vegetation changes over the last 45k cal a BP in the uplands of south-eastern Amazonia. *J. Quat. Sci.* **2021**, *36*, 255–272. [[CrossRef](#)]
18. Reis, L.S.; Bouloubassi, I.; Mendez-Millan, M.; Guimarães, J.T.F.; Romeiro, L.D.A.; Sahoo, P.K.; Pessenda, L.C.R. Hydroclimate and vegetation changes in southeastern Amazonia over the past ~25,000 years. *Quat. Sci. Rev.* **2022**, *284*, 107466. [[CrossRef](#)]
19. Lopes, P.M.; Caliman, A.; Carneiro, L.S.; Bini, L.M.; Esteves, F.A.; Farjalla, V.; Bozelli, R.L. Concordance among assemblages of upland Amazonian lakes and the structuring role of spatial and environmental factors. *Ecol. Indic.* **2011**, *11*, 1171–1176. [[CrossRef](#)]
20. Mormul, R.P.; Esteves, F.D.A.; Farjalla, V.F.; Bozelli, R.L. Space and seasonality effects on the aquatic macrophyte community of temporary Neotropical upland lakes. *Aquat. Bot.* **2015**, *126*, 54–59. [[CrossRef](#)]
21. Silva, M.S.; Guimarães, J.T.F.; Souza Filho, P.W.M.; Nascimento Júnior, W.R.; Sahoo, P.K.; Costa, F.R.; Silva Júnior, R.O.; Rodrigues, T.M.; Costa, M.F. Morphology and morphometry of upland lakes over lateritic crust, Serra dos Carajás, southeastern Amazon region. *An. Acad. Bras. Ciências* **2018**, *90*, 1309–1325. [[CrossRef](#)]
22. Schnurrenberger, D.; Russell, J.; Kelts, K. Classification of lacustrine sediments based on sedimentary components. *J. Paleolimnol.* **2003**, *29*, 141–154. [[CrossRef](#)]
23. Walker, R.G. Facies, facies models and modern stratigraphic concepts. In *Facies Models—Response to Sea Level Change*, 2nd ed.; Walker, R.G., James, N.P., Eds.; Geological Association of Canada: Toronto, ON, Canada, 1992; pp. 1–14.
24. Moraes, A.M.; Sahoo, P.K.; Guimarães, J.T.F.; Leite, A.S.; Salomão, G.N.; Souza-Filho, P.W.M.; Júnior, W.N.; Dall'Agnol, R. Multivariate statistics and geochemical approaches for understanding source-sink relationship—A case study from close-basin lakes in Southeast Amazon. *J. S. Am. Earth Sci.* **2020**, *99*, 102497. [[CrossRef](#)]
25. Sahoo, P.K.; Guimarães, J.T.F.; Souza-Filho, P.W.M.; Powell, M.A.; da Silva, M.S.; Moraes, A.M.; Alves, R.; Leite, A.S.; Júnior, W.N.; Rodrigues, T.M.; et al. Statistical analysis of lake sediment geochemical data for understanding surface geological factors and processes: An example from Amazonian upland lakes, Brazil. *Catena* **2018**, *175*, 47–62. [[CrossRef](#)]
26. Guimarães, J.T.G.; Sahoo, P.; Souza-Filho, P.W.M.; Silva, M.; Rodrigues, T.; Silva, E.; Reis, L.; Figueiredo, M.; Lopes, K.; Batista Junior, W.; et al. Upland Lakes of the Carajás Region: Origin and Development through Time. *Preprints* **2019**, 2019050214. [[CrossRef](#)]
27. Guimarães, J.T.; Sahoo, P.K.; Souza-Filho, P.W.; DE Figueiredo, M.M.C.; Reis, L.S.; Da Silva, M.S.; Rodrigues, T.M. Holocene history of a lake filling and vegetation dynamics of the Serra Sul dos Carajás, southeast Amazonia. *An. Acad. Bras. Ciênc.* **2019**, *91*, e20160916. [[CrossRef](#)]
28. Da Silva, E.F.; Lopes, K.D.S.; Alves, R.; Carreira, L.M.M.; da Silva, D.F.; Romeiro, L.D.A.; Júnior, W.F.B.; Rodrigues, T.M.; Secco, R.D.S.; Guimarães, J.T.F. Hydroclimate influences on modern pollen rain of upland southeastern Amazonia. *Holocene* **2020**, *30*, 721–732. [[CrossRef](#)]

29. Guimarães, J.T.F.; Souza-Filho, P.W.M.; Alves, R.; Souza, E.B.; Costa, F.R.; Reis, L.S.; Sahoo, P.K.; Manes, C.L.O.; Silva Junior, R.O.; Oti, D.; et al. Source and distribution of pollen and spores in surface sediments of a plateau lake in south-eastern Amazonia. *Quat. Int.* **2014**, *352*, 181–196. [[CrossRef](#)]
30. Guimarães, J.T.F.; Rodrigues, T.M.R.; Reis, L.S.; de Figueiredo, M.M.J.C.; da Silva, D.F.; Alves, R.; Giannini, T.C.; Carreira, L.M.M.; Dias, A.C.R.; Silva, E.F.; et al. Modern pollen rain as a background for palaeoenvironmental studies in the Serra dos Carajás, southeastern Amazonia. *Holocene* **2017**, *27*, 1055–1066. [[CrossRef](#)]
31. Faegri, K.; Iversen, J. *Textbook of Pollen Analyses*; Wiley: Chichester, UK, 1989.
32. Blaauw, M.; Christen, J.A. Flexible palaeoclimate age-depth models using an autoregressive gamma process. *Bayesian Anal.* **2011**, *6*, 457–474. [[CrossRef](#)]
33. Reimer, P.J.; Austin, W.E.N.; Bard, E.; Bayliss, A.; Blackwell, P.G.; Ramsey, C.B.; Butzin, M.; Cheng, H.; Edwards, R.L.; Friedrich, M.; et al. The IntCal20 Northern Hemisphere Radiocarbon Age Calibration Curve (0–55 cal kBP). *Radiocarbon* **2020**, *62*, 725–757. [[CrossRef](#)]
34. EPA. *Method 9060A—Total Organic Carbon. 5P. Revision 1*; United States Environmental Protection Agency: Washington, DC, USA, 2004.
35. SMEWW. *1060—Collection and Preservation of Samples; Standard Methods for the Examination of Water and Wastewater*: Washington, DC, USA, 2005.
36. Feio, G.; Dall’Agnol, R.; Dantas, E.; Macambira, M.; Santos, J.; Althoff, F.; Soares, J. Archean granitoid magmatism in the Canaã dos Carajás area: Implications for crustal evolution of the Carajás province, Amazonian craton, Brazil. *Precambrian Res.* **2013**, *227*, 157–185. [[CrossRef](#)]
37. Moreto, C.P.N.; Monteiro, L.V.S.; Xavier, R.P.; Creaser, R.A.; DuFrane, S.A.; Tassinari, C.C.G.; Sato, K.; Kemp, A.I.S.; Amaral, W.S. Neoproterozoic Iron Oxide–Copper–Gold Events at the Sossego Deposit, Carajás Province, Brazil: Re-Os and U–Pb Geochronological Evidence. *Econ. Geol.* **2015**, *110*, 809–835. [[CrossRef](#)]
38. Martins, P.L.G.; Toledo, C.L.B.; Silva, A.M.S.; Chemale, F., Jr.; Santos, J.O.S.; Assis, L.M. Neoproterozoic magmatism in the southeastern Amazonian Craton, Brazil: Petrography, geochemistry and tectonic significance of basalts from the Carajás Basin. *Precambrian Res.* **2017**, *302*, 340–357. [[CrossRef](#)]
39. Dall’Agnol, R.; da Cunha, I.R.V.; Guimarães, F.V.; de Oliveira, D.C.; Teixeira, M.F.B.; Feio, G.R.L.; Lamarão, C.N. Mineralogy, geochemistry, and petrology of Neoproterozoic ferroan to magnesian granites of Carajás Province, Amazonian Craton: The origin of hydrated granites associated with charnockites. *Lithos* **2017**, *277*, 3–32. [[CrossRef](#)]
40. Mansur, E.T.; Filho, C.F.F.; Oliveira, D.P. The Luanga deposit, Carajás Mineral Province, Brazil: Different styles of PGE mineralization hosted in a medium-size layered intrusion. *Ore Geol. Rev.* **2020**, *118*, 103340. [[CrossRef](#)]
41. Nogueira, A.C.R.; Trunckenbrodt, W.; Pinheiro, R.L.V. Formação Águas Claras, Pré-cambriano da Serra dos Carajás: Redescoberta e redefinição litoestratigráfica. *Bol. Mus. Para. Emílio Goeldi* **1995**, *7*, 177–197.
42. Dall’Agnol, R.; Teixeira, N.P.; Rämö, O.T.; Moura, C.A.; Macambira, M.J.; de Oliveira, D.C. Petrogenesis of the Paleoproterozoic rapakivi A-type granites of the Archean Carajás metallogenic province, Brazil. *Lithos* **2005**, *80*, 101–129. [[CrossRef](#)]
43. Vasquez, M.L.; Sousa, C.S.; Carvalho, K.M.A. *Mapa Geológico e de Recursos Minerais do Estado do Pará, escala 1:1.000.000. Programa Geologia do Brasil (PGB), Integração, Atualização e Difusão de Dados da Geologia do Brasil, Mapas Geológicos Estaduais*; Serviço Geológico do Brasil (CPRM): Sao Paulo, Brazil, 2008.
44. Souza-Filho, P.W.M.; Guimarães, J.T.F.; Silva, M.S.; Costa, F.R.; Sahoo, P.K.; Maurity, C.W.; Dall’Agnol, R. Basin morphology, sedimentology and seismic stratigraphy of an upland lake from Serra dos Carajás, southeastern Amazon, Brazil. *Bol. Mus. Para. Emílio Goeldi. Cienc. Nat.* **2016**, *11*, 71–83. [[CrossRef](#)]
45. Lopes, M.N.G.; Souza, E.B.; Ferreira, D.B.D.S. Climatologia regional da precipitação no estado do Pará. *Rev. Bras. Climatol.* **2013**, *12*, 84–102.
46. Da Silva Júnior, R.O.; De Souza, E.B.; Tavares, A.L.; Mota, J.A.; Ferreira, D.B.; Souza-Filho, P.W.; Da Rocha, E.J. Three decades of reference evapotranspiration estimates for a tropical watershed in the eastern Amazon. *An. Acad. Bras. Ciências* **2017**, *89*, 1985–2002. [[CrossRef](#)]
47. Tavares, A.L.; Carmo, A.M.C.; Silva Júnior, R.O.; Souza-Filho, P.W.M.; Silva, M.S.; Ferreira, D.B.S.; Nascimento Júnior, W.R.; Dall’Agnol, R. Climate indicators for a watershed in the eastern Amazon. *Rev. Bras. Climatol.* **2018**, *23*, 389–410. [[CrossRef](#)]
48. Golder. Anexo IV—Geologia. Estudo de Impacto Ambiental, EIA Projeto Ferro Carajás S11D. 2010. Available online: http://licenciamento.ibama.gov.br/Mineracao/Projeto%20Ferro%20Carajas%20S11D/EIA_RIMA/ (accessed on 13 April 2014).
49. Skirycz, A.; Castilho, A.; Chaparro, C.; Carvalho, N.; Tzotzos, G.; Siqueira, J.O. Canga biodiversity, a matter of mining. *Front. Plant Sci.* **2014**, *5*, 653. [[CrossRef](#)]
50. Schaefer, C.G.R.E.; Lima Neto, E.; Corrêa, G.R.; Simas, F.N.B.; Campos, J.F.; De Mendonça, B.A.F. Geoenvironments, soils and carbon stocks at Serra Sul of Carajás, Para State, Brazil. *Bol. Mus. Para. Emílio Goeldi Cienc. Nat.* **2016**, *11*, 85–101. [[CrossRef](#)]
51. Mitre, S.K.; Mardegan, S.F.; Caldeira, C.F.; Ramos, S.J.; Neto, A.E.F.; Siqueira, J.O.; Gastauer, M. Nutrient and water dynamics of Amazonian canga vegetation differ among physiognomies and from those of other neotropical ecosystems. *Plant Ecol.* **2018**, *219*, 1341–1353. [[CrossRef](#)]
52. Caldeira, C.F.; Abranches, C.B.; Gastauer, M.; Ramos, S.J.; Guimarães, J.T.F.; Pereira, J.B.S.; Siqueira, J.O. Sporeling regeneration and ex situ growth of *Isoetes cangae* (Isoetaceae): Initial steps towards the conservation of a rare Amazonian quillwort. *Aquat. Bot.* **2018**, *152*, 51–58. [[CrossRef](#)]

53. Viana, P.L.; Mota, N.F.O.; Gil, A.S.B.; Salino, A.; Zappi, D.C.; Harley, R.M.; Ilkiu-Borges, A.L.; Secco, R.; Almeida, T.E.; Watanabe, M.T.C.; et al. Flora of the cangas of the Serra dos Carajás, Pará, Brazil: History, study area and methodology. *Rodriguesia* **2016**, *67*, 1107–1124. [[CrossRef](#)]
54. Wetzel, R.G. (Ed.) Oxygen. In *Limnology*; Academic Press: London, UK, 2001; pp. 151–168.
55. Deines, P. The isotopic composition of reduced organic carbon. In *Handbook of Environmental Isotope Geochemistry e the Terrestrial Environment*; Fritz, P., Fontes, J.C., Eds.; Elsevier: Amsterdam, The Netherlands, 1980; pp. 329–406.
56. Boutton, T.W. Stable carbon isotope ratios of natural materials: II. Atmospheric, terrestrial, marine, and freshwater environments. In *Carbon Isotope Techniques*; Coleman, D.C., Fry, B., Eds.; Academic Press Inc.: New York, NY, USA, 1991; pp. 173–185.
57. Hamilton, S.K.; Lewis, W.M., Jr. Stable carbon and nitrogen isotopes in algae and detritus from the Orinoco River floodplain, Venezuela. *Geochim. Cosmochim. Acta* **1992**, *56*, 4237–4246. [[CrossRef](#)]
58. Thornton, S.; McManus, J. Application of Organic Carbon and Nitrogen Stable Isotope and C/N Ratios as Source Indicators of Organic Matter Provenance in Estuarine Systems: Evidence from the Tay Estuary, Scotland. *Estuar. Coast. Shelf Sci.* **1994**, *38*, 219–233. [[CrossRef](#)]
59. Meyers, P.A. Organic geochemical proxies of paleoceanographic, paleolimnologic, and paleoclimatic processes. *Org. Geochem.* **1997**, *27*, 213–250. [[CrossRef](#)]
60. Brenner, M.; Whitmore, T.J.; Curtis, J.H.; Hodell, D.; Schelske, C.L. Stable isotope ($\delta^{13}\text{C}$ and $\delta^{15}\text{N}$) signatures of sedimented organic matter as indicators of historic lake trophic state. *J. Paleolimnol.* **1999**, *22*, 205–221. [[CrossRef](#)]
61. Troxler, T.G.; Richards, J.H. $\delta^{13}\text{C}$, $\delta^{15}\text{N}$, carbon, nitrogen and phosphorus as indicators of plant ecophysiology and organic matter pathways in Everglades deep slough, Florida, USA. *Aquat. Bot.* **2009**, *91*, 157–165. [[CrossRef](#)]
62. Smith, C.B.; Cohen, M.C.L.; Pessenda, L.; França, M.; Guimarães, J. Holocene proxies of sedimentary organic matter and the evolution of Lake Arari-Amazon Region. *CATENA* **2011**, *90*, 26–38. [[CrossRef](#)]
63. Guimarães, J.T.F.; Sahoo, P.; Reis, L.S. Modern pollen rain raises doubts about the intensity and extension of the Last Glacial Cycle in Carajás: A reply to D’Apolito et al. *Holocene* **2017**, *28*, 332–335. [[CrossRef](#)]
64. Pereira, J.B.D.S.; Salino, A.; Arruda, A.; Stützel, T. Two New Species of Isoetes (Isoetaceae) from northern Brazil. *Phytotaxa* **2016**, *272*, 141–148. [[CrossRef](#)]
65. De Oliveira, S.M.B.; Saia, S.E.M.G.; Pessenda, L.C.R.; Favaro, D.I.T. Lacustrine sediments provide geochemical evidence of environmental change during the last millennium in southeastern Brazil. *Geochemistry* **2009**, *69*, 395–405. [[CrossRef](#)]
66. Hodell, D.A.; Schelske, C.L. Production, sedimentation, and isotopic composition of organic matter in Lake Ontario. *Limnol. Oceanogr.* **1998**, *43*, 200–214. [[CrossRef](#)]
67. Zhang, Y.; Zhang, X.; Chiessi, C.M.; Mulitza, S.; Zhang, X.; Lohmann, G.; Prange, M.; Behling, H.; Zabel, M.; Govin, A.; et al. Equatorial Pacific forcing of western Amazonian precipitation during Heinrich Stadial 1. *Sci. Rep.* **2016**, *6*, 35866. [[CrossRef](#)] [[PubMed](#)]
68. Fontes, D.; Cordeiro, R.; Martins, G.; Behling, H.; Turcq, B.; Sifeddine, A.; Seoane, J.; Moreira, L.; Rodrigues, R. Paleoenvironmental dynamics in South Amazonia, Brazil, during the last 35,000 years inferred from pollen and geochemical records of Lago do Saci. *Quat. Sci. Rev.* **2017**, *173*, 161–180. [[CrossRef](#)]
69. Kimberley, M.M. Exhalative origins of iron formations. *Ore Geol. Rev.* **1989**, *5*, 13–145. [[CrossRef](#)]
70. Lemos, V.P.; Costa, M.L.C.; Lemos, R.L.; de Faria, M.S.G. Vivianite and siderite in lateritic iron crust: An example of bioreduction. *Quim. Nova* **2007**, *30*, 36–40. [[CrossRef](#)]
71. Maslin, M.A.; Ettwein, V.J.; Boot, C.S.; Bendle, J.; Pancost, R.D. Amazon Fan biomarker evidence against the Pleistocene rainforest refuge hypothesis? *J. Quat. Sci.* **2012**, *27*, 451–460. [[CrossRef](#)]
72. Häggi, C.; Chiessi, C.M.; Merkel, U.; Mulitza, S.; Prange, M.; Schulz, M.; Schefuß, E. Response of the Amazon rainforest to late Pleistocene climate variability. *Earth Planet. Sci. Lett.* **2017**, *479*, 50–59. [[CrossRef](#)]
73. Wang, X.; Edwards, R.L.; Auler, A.S.; Cheng, H.; Kong, X.; Wang, Y.; Cruz, F.W.; Dorale, J.A.; Chiang, H.-W. Hydroclimate changes across the Amazon lowlands over the past 45,000 years. *Nature* **2017**, *541*, 204–207. [[CrossRef](#)] [[PubMed](#)]
74. Absy, M.L.; Cleef, A.M.; Fournier, M.; Martin, L.; Servant, M.; Sifeddine, A.; Silva da Soubiès, F.; Suguio, K.; Turcq, B.J.; Van der Hammen, T. Mise en évidence de quatre phases d’ouverture de la forêt dense dans le Sud-Est de l’Amazonie au cours des 60,000 dernières années: Première comparaison avec d’autres régions tropicales. *Comptes Rendus L’académie Sci.* **1991**, *312*, 673–678.
75. Cordeiro, R.C.; Turcq, B.; Suguio, K.; Oliveira da Silva, A.; Sifeddine, A.; Volkmer, C. Holocene fires in East Amazonia (Carajás), new evidences, chronology and relation with palaeoclimate. *Glob. Planet. Change* **2008**, *61*, 49–62. [[CrossRef](#)]
76. Hermanowski, B.; Da Costa, M.L.; Behling, H. Possible linkages of palaeofires in southeast Amazonia to a changing climate since the Last Glacial Maximum. *Veg. Hist. Archaeobot.* **2014**, *24*, 279–292. [[CrossRef](#)]
77. Smith, R.J.; Mayle, F.E. Impact of mid- to late Holocene precipitation changes on vegetation across lowland tropical South America: A paleo-data synthesis. *Quat. Res.* **2017**, *89*, 134–155. [[CrossRef](#)]
78. Cross, S.L.; Baker, P.A.; Seltzer, G.O.; Fritz, S.C.; Dunbar, R.B. A new estimate of the Holocene lowstand level of Lake Titicaca, central Andes, and implications for tropical palaeohydrology. *Holocene* **2000**, *10*, 21–32. [[CrossRef](#)]
79. Seltzer, G.; Rodbell, D.; Burns, S. Isotopic evidence for late Quaternary climatic change in tropical South America. *Geology* **2000**, *28*, 35–38. [[CrossRef](#)]
80. Mayle, F.E.; Power, M.J. Impact of a drier Early–Mid-Holocene climate upon Amazonian forests. *Philos. Trans. R. Soc. B Biol. Sci.* **2008**, *363*, 1829–1838. [[CrossRef](#)]

81. Guimarães, J.T.F.; Cohen, M.C.L.; Pessenda, L.C.R.; França, M.C.; Smith, C.B.; Nogueira, A.C.R. Mid and late Holocene sedimentary process and palaeovegetation changes near the mouth of the Amazon River. *Holocene* **2012**, *22*, 359–370. [[CrossRef](#)]
82. Prado, L.F.; Wainer, I.; Chiessi, C.M.; Ledru, M.-P.; Turcq, B. A mid-Holocene climate reconstruction for eastern South America. *Clim. Past* **2013**, *9*, 2117–2133. [[CrossRef](#)]
83. Maksic, J.; Shimizu, M.H.; De Oliveira, G.S.; Venancio, I.; Cardoso, M.; Ferreira, F.A. Simulation of the Holocene climate over South America and impacts on the vegetation. *Holocene* **2018**, *29*, 287–299. [[CrossRef](#)]
84. Sifeddine, A.; Frohlich, F.; Fournier, M.; Martin, L.; Servant, M.; Soubiès, F.; Turcq, B.; Suguio, K.; Volkmer-Ribeiro, C. La sédimentation lacustre indicateur de changements des paléoenvironnements au cours des 30 000 dernières années (Caraias, Amazonie, Brésil). *Académie Sci. Paris* **1994**, *318*, 1645–1652.
85. Pinakhina, D.V.; Chekunova, E.M. Environmental DNA: History of studies, current and perspective applications in fundamental and applied research. *Ecol. Genet.* **2020**, *18*, 493–509. [[CrossRef](#)]
86. Thomsen, P.F.; Willerslev, E. Environmental DNA—An emerging tool in conservation for monitoring past and present biodiversity. *Biol. Conserv.* **2015**, *183*, 4–18. [[CrossRef](#)]
87. Bohmann, K.; Evans, A.; Gilbert, M.T.P.; Carvalho, G.R.; Creer, S.; Knapp, M.; Yu, D.W.; De Bruyn, M. Environmental DNA for wildlife biology and biodiversity monitoring. *Trends Ecol. Evol.* **2014**, *29*, 358–367. [[CrossRef](#)] [[PubMed](#)]
88. Haile, J.; Holdaway, R.; Oliver, K.; Bunce, M.; Gilbert, M.; Nielsen, R.; Munch, K.; Ho, S.Y.W.; Shapiro, B.; Willerslev, E. Ancient DNA Chronology within Sediment Deposits: Are Paleobiological Reconstructions Possible and Is DNA Leaching a Factor? *Mol. Biol. Evol.* **2007**, *24*, 982–989. [[CrossRef](#)] [[PubMed](#)]
89. Willerslev, E.; Hansen, A.J.; Binladen, J.; Brand, T.B.; Gilbert, M.T.P.; Shapiro, B.; Bunce, M.; Wiuf, C.; Gilichinsky, D.A.; Cooper, A. Diverse Plant and Animal Genetic Records from Holocene and Pleistocene Sediments. *Science* **2003**, *300*, 791–795. [[CrossRef](#)]
90. Yoccoz, N.; Bråthen, K.A.; Gielly, L.; Haile, J.; Edwards, M.E.; Goslar, T.; Von Stedingk, H.; Brysting, A.K.; Coissac, E.; Pompanon, F.; et al. DNA from soil mirrors plant taxonomic and growth form diversity. *Mol. Ecol.* **2012**, *21*, 3647–3655. [[CrossRef](#)] [[PubMed](#)]
91. Giguët-Covex, C.; Pansu, J.; Arnaud, F.; Rey, P.-J.; Griggo, C.; Gielly, L.; Domaizon, I.; Coissac, E.; David, F.; Choler, P.; et al. Long livestock farming history and human landscape shaping revealed by lake sediment DNA. *Nat. Commun.* **2014**, *5*, 3211. [[CrossRef](#)] [[PubMed](#)]
92. Correa-Metrio, A.; Bush, M.B.; Cabrera, K.R.; Sully, S.; Brenner, M.; Hodell, D.A.; Escobar, J.; Guilderson, T. Rapid climate change and no-analog vegetation in lowland Central America during the last 86,000 years. *Quat. Sci. Rev.* **2012**, *38*, 63–75. [[CrossRef](#)]
93. Correa-Metrio, A.; Urrego, D.H.; Cabrera, K.R.; Bush, M.B. PaleoMAS: Paleo-ecological Analysis, R Package Version 2.0-1 ed. The R Project for Statistical Computing. 2011. Available online: <http://CRAN.R-project.org/package=paleoMAS> (accessed on 20 February 2019).
94. Holtvoeth, J.; Whiteside, J.H.; Engels, S.; Freitas, F.S.; Grice, K.; Greenwood, P.; Johnson, S.; Kendall, I.; Lengger, S.K.; Lücke, A.; et al. The paleolimnologist's guide to compound-specific stable isotope analysis—An introduction to principles and applications of CSIA for Quaternary lake sediments. *Quat. Sci. Rev.* **2019**, *207*, 101–133. [[CrossRef](#)]
95. Sachse, D.; Billault, I.; Bowen, G.J.; Chikaraishi, Y.; Dawson, T.E.; Feakins, S.J.; Freeman, K.H.; Magill, C.R.; McNerney, F.A.; van der Meer, M.T.; et al. Molecular Paleohydrology: Interpreting the Hydrogen-Isotopic Composition of Lipid Biomarkers from Photosynthesizing Organisms. *Annu. Rev. Earth Planet. Sci.* **2012**, *40*, 221–249. [[CrossRef](#)]
96. Piló, L.B.; Auler, A.S.; Martins, F. Carajás National Forest: Iron Ore Plateaus and Caves in Southeastern Amazon. In *Landscapes and Landforms of Brazil, World Geomorphological Landscapes*; Vieira, B.C., Salgado, A.A.R., Santos, L.J.C., Eds.; Springer: Berlin/Heidelberg, Germany, 2015; pp. 273–283.
97. Piló, L.B.; Calux, A.; Scherer, R.; Bernard, E. Bats as ecosystem engineers in iron ore caves in the Carajás National Forest, Brazilian. *bioRxiv* **2022**. [[CrossRef](#)]
98. Bird, M.I.; Boobyer, E.M.; Bryant, C.; Lewis, H.A.; Paz, V.; Stephens, W.E. A long record of environmental change from bat guano deposits in Makangit Cave, Palawan, Philippines. *Earth Environ. Sci. Trans. R. Soc. Edinb.* **2007**, *98*, 59–69. [[CrossRef](#)]
99. Widga, C.; Colburn, M. Paleontology and paleoecology of guano deposits in Mammoth Cave, Kentucky, USA. *Quat. Res.* **2015**, *83*, 427–436. [[CrossRef](#)]
100. Wurster, C.; McFarlane, D.; Bird, M.; Ascough, P.; Athfield, N.B. Stable Isotopes of Subfossil Bat Guano as a Long-Term Environmental Archive: Insights from a Grand Canyon Cave Deposit. *J. Cave Karst Stud.* **2010**, *72*, 111–121. [[CrossRef](#)]
101. Wurster, C.; Patterson, W.; McFarlane, D.A.; Wassenaar, L.; Hobson, K.A.; Athfield, N.B.; Bird, M. Stable carbon and hydrogen isotopes from bat guano in the Grand Canyon, USA, reveal Younger Dryas and 8.2 ka events. *Geology* **2008**, *36*, 683. [[CrossRef](#)]

Disclaimer/Publisher's Note: The statements, opinions and data contained in all publications are solely those of the individual author(s) and contributor(s) and not of MDPI and/or the editor(s). MDPI and/or the editor(s) disclaim responsibility for any injury to people or property resulting from any ideas, methods, instructions or products referred to in the content.